

1-1-1990

Gas dynamics in interacting and merging galaxies.

Kevin Mark Olson

University of Massachusetts Amherst

Follow this and additional works at: https://scholarworks.umass.edu/dissertations_1

Recommended Citation

Olson, Kevin Mark, "Gas dynamics in interacting and merging galaxies." (1990). *Doctoral Dissertations 1896 - February 2014*. 1795.
https://scholarworks.umass.edu/dissertations_1/1795

This Open Access Dissertation is brought to you for free and open access by ScholarWorks@UMass Amherst. It has been accepted for inclusion in Doctoral Dissertations 1896 - February 2014 by an authorized administrator of ScholarWorks@UMass Amherst. For more information, please contact scholarworks@library.umass.edu.

312066007491840

GAS DYNAMICS IN INTERACTING AND MERGING GALAXIES

A Dissertation Presented

by

KEVIN MARK OLSON

Submitted to the Graduate School of the
University of Massachusetts in partial fulfillment
of the requirements for the degree of

DOCTOR OF PHILOSOPHY

February 1990

Department of Physics and Astronomy

© Copyright by Kevin Mark Olson 1990
All rights reserved

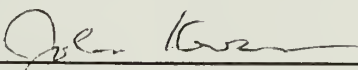
GAS DYNAMICS IN INTERACTING AND MERGING GALAXIES

A Dissertation Presented

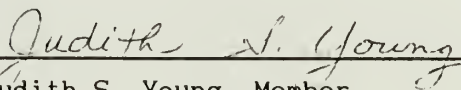
by

KEVIN MARK OLSON

Approved as to style and content by:



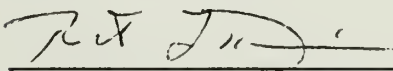
John Kwan, Chair



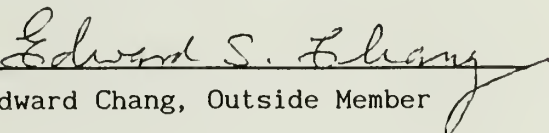
Judith S. Young, Member




Susan G. Kleinmann, Member



Robert Dickman, Member



Edward Chang, Outside Member



Robert B. Hallock, Department Head
Department of Physics and Astronomy

DEDICATION

To the memory of my father,

David G. Olson.

ACKNOWLEDGEMENTS

First and foremost I wish to thank my advisor, John Kwan, for providing the necessary theoretical expertise for the solution of the problem at hand and for his no nonsense approach to this project. In developing large computer codes its always a temptation to believe the results when they first appear. John taught me, more than anything else, to resist this temptation and to be conservative.

Secondly, I thank Judy Young for providing a great deal of enthusiasm for the work I was doing. I also thank her for helping me to understand some of the observational aspects of the problem and for introducing me to the observational peculiarities of interacting galaxies. Thanks go also to the other members of my committee, Susan Kleinmann and Bob Dickman.

Most of the calculations in this work were performed at the Cornell National Supercomputer Facility. I am especially grateful to Robert Gonter and Kurt Gordon, the consultants here at U. Mass., who introduced me to CNSF and for helping me at all stages in the computations. Hugh Caffey and all the CNSF consultants who answered my questions deserve special thanks. All the people I was involved with in connection with CNSF did an excellent job and always did it in a polite manner.

I also wish to thank Nick Devereaux and Steve Lord for taking and interest in this project and providing useful comments and advice. José Alonso-Costa and Jim Morgan are acknowledged for philosophical discussions.

Last, but certainly not least, I thank my family for providing the love, support, and encouragement I needed to get things done.

ABSTRACT

GAS DYNAMICS IN INTERACTING AND MERGING GALAXIES

FEBRUARY 1990

KEVIN MARK OLSON, B.S., THE PENNSYLVANIA STATE UNIVERSITY

Ph.D., UNIVERSITY OF MASSACHUSETTS

Directed by: Professor John Kwan

In this dissertation I develop a three dimensional model of the dynamics of gas clouds in interacting galaxies. The gas clouds move under the combined gravitational influence of two galaxies passing close to each other. By performing a multipole expansion of the gravitational field I am able to include the effects of self-gravity within a galaxy. This also allows me to model the case in which the two galaxies merge. The gas clouds are allowed to interact with one another by colliding. They either coalesce to form a larger cloud or are disrupted, depending on their relative kinetic energy as compared to the total gravitational binding energy of the two-cloud system. Various cases are considered in this dissertation by varying such parameters as impact parameter, inclination of the gaseous disk of a galaxy to the orbital plane of the two, interacting galaxies, relative velocity of the galaxies, the mass ratio of the galaxies, and the presence of gas in the second galaxy. As the strength of the interaction increases the more disturbed the interstellar medium becomes. The clouds collide at an increased rate and with larger velocities so that the fraction of collisions which disrupt the clouds rises as the strength of the interaction increases. The region of the galaxy where increased rates of collision are induced also becomes more and more concentrated toward the center of the

galaxy. Since interacting galaxies are observed to have elevated star formation rates, I conclude that the star formation induced by the interaction of two galaxies is related to the high velocity, disruptive cloud-cloud collisions. Monitoring the amount of gas mass involved in such collisions allows me to estimate the star formation rate and the luminosity produced by these stars. Considering parameters such as inclination, bound and unbound orbits, the mass of the perturbing galaxy, and the possible presence of gas in both galaxies, I find that the scatter in observations of the infrared luminosity to gas mass ratio can be explained.

TABLE OF CONTENTS

	Page
ACKNOWLEDGEMENTS	v
ABSTRACT	vi
LIST OF TABLES	ix
LIST OF FIGURES	x
Chapter	
1 INTRODUCTION	1
2 MODEL	8
2.1 Gravitational Field Calculation	8
2.2 Cloud-Cloud Collisions	11
3 VARIATIONS WITH IMPACT PARAMETER	18
3.1 Results	18
3.1.1 $b = 60$ kpc	18
3.1.2 $b = 40$ kpc	22
3.1.3 $b = 20$ kpc	30
3.2 Discussion	37
3.2.1 Cloud-Cloud Collisions and Star Formation	40
3.2.2 Luminosity to Gas Mass Ratio	45
3.2.3 Comparisons with Other Theories	49
4 VARIATIONS WITH OTHER PARAMETERS	54
4.1 Results	54
4.2 Discussion	77
5 SUMMARY	90
BIBLIOGRAPHY	93

LIST OF TABLES

Page

1 Parameters for all Models56

LIST OF FIGURES

		Page
1	The morphological change of the cloud system for case 1 ...	19
2	Time dependences, in the region exterior to 2 kpc of the galactic center, of the total rate of cloud-cloud collision (in units of number per 10 Myr), the rate of coalescence, the rate of large collisional disruptions, and the rate at which fragments are produced due to star formation in massive clouds	21
3	Same as Fig. 2 except for the region interior to 2 kpc	23
4	The distribution of collisional velocities before the time of closest approach and at the time of peak total collisional rate after closest approach	24
5	Same as Fig. 1 except for case 2	25
6	Same as Fig. 2 except for case 2, i.e. the region exterior to 2 kpc	26
7	Same as Fig. 3 except for case 2, i.e. the region interior to 2 kpc	27
8	Same as Fig. 4 except for case 2	29
9	Plots of $2\pi r\sigma$ vs. radius at different times in case 2	31
10	Face-on view of the morphological change of the cloud system in case 3 where the galaxies merge	33
11	Edge-on view of the cloud system for case 3 showing the large motions induced perpendicular to the original disk of the galaxy	34
12	Same as Fig. 2 except for case 3, i.e. the region exterior to 2 kpc	35
13	Same as Fig. 3 except for case 3, i.e. the region interior to 2 kpc	36
14	Same as Fig. 4 except for case 3	38
15	Same as Fig. 9 except for case 3	39
16	The rate at which mass is involved in large disruptive and glancing collisions as a function of time in case 2 ...	44

17	The time dependences of the stellar luminosity produced by the galaxy-galaxy interaction in case 2 for three values of the power law index of the initial stellar mass function	46
18	The morphological change of the cloud system for case 4 ($i = 120^\circ$)	57
19	Time dependences for case 4, in the region exterior to 2 kpc of the galactic center, of the total rate of cloud-cloud collision (in units of number per 10 Myr), the rate of coalescence, the rate of large collisional disruptions, and the rate at which fragments are produced due to star formation in massive clouds	58
20	Same as Fig. 18 except for case 5 ($i = 30^\circ$, $b = 40$ kpc, and $\gamma = 2$)	60
21	Same as Fig. 19 except for case 5	61
22	Face-on view of the morphological change of the cloud system in case 6 ($i = 30^\circ$, $b = 40$ kpc, and $\gamma = 1/2$) where the galaxies merge	63
23	Edge-on view of the cloud system for case 6	64
24	Same as Fig. 19 except plots are for the region interior to 2 kpc for case 6	66
25	Same as Fig. 18 except for case 7 (perturber mass is $1/2$ galaxy mass)	69
26	Same as Fig. 19 except for case 7	70
27	Same as Fig. 24 (region less than 2 kpc) except for case 7	71
28	Same as Fig. 18 except for case 8	72
29	Same as Fig. 23 except for case 8	73
30	Same as Fig. 24 (region less than 2 kpc) except for case 8	75
31	Distributions of the relative velocities of the cloud-cloud collisions at four different times for case 8	76
32	The luminosity to gas mass ratio as function of time for case 6 with $\epsilon = 20\%$ taking into account the depletion of gas due to star formation for $\alpha = 2.45$, 1.45, and 0.45	82

33 The luminosity of the galaxies as a function of time
for case 8 where both galaxies contain gas85

34 The luminosity to gas mass ratio as a function of time
for case 8 taking into account the depletion of gas due
to star formation86

35 The luminosity to gas mass ratio as a function of time
for case 9 where the total amount of gas is one half
that in case 8 and both galaxies contain gas88

CHAPTER 1

INTRODUCTION

The close passage of two galaxies and their subsequent gravitational interaction has been shown to produce the dramatic bridges and tails associated with close pairs of galaxies (Toomre and Toomre 1972). More recently it has been suggested that an interaction can lead to a burst of star formation in one or both of the galaxies. Larson and Tinsley (1978) show that the galaxies in Arp's atlas (1966) have a wider dispersion on the U-B vs. B-V color-color diagram than non-interacting galaxies. Through the use of simple spectral energy distribution models for the stars in a galaxy, they show that this dispersion can be brought about by a burst of star formation. More compelling evidence that interacting galaxies have elevated star formation rates has come from infrared observations. Joseph and Wright (1985) have shown that known cases of interacting galaxies have infrared luminosities at $10\ \mu\text{m}$ that are higher than average. A similar result for the luminosity between 1 and $10\ \mu\text{m}$ is obtained by Lonsdale, Persson and Mathews (1984). They take this as evidence that young stars, formed in a burst triggered by the interaction of two galaxies, are heating the dust surrounding them, causing reradiation of the absorbed stellar photons in the infrared. Similar results are obtained when considering the far infrared continuum of interacting galaxies (e.g. Bushouse, Lamb, and Werner 1988 and Smith 1988).

The properties of the ionized gas in interacting galaxies also show evidence for enhanced star formation. Bushouse (1986), using a sample of interacting galaxies with clear morphological disturbances (e.g., tidal tails and bridges), finds that most of these galaxies show enhancements in their H α fluxes only near the nuclei of the galaxies, but that there are also galaxies which show enhancements in their H α fluxes in their disks with no detectable H α flux near their centers. Bushouse (1986) also shows that the optical spectra of the interacting galaxies in his sample are consistent with that produced by gas ionized by a stellar continuum rather than by an active nucleus or shocks. In a similar study Kennicutt and Keel (1984) and Kennicutt et al. (1987) show that the galaxies which are the most morphologically disturbed are the ones having the highest rates of star formation. Also, Kennicutt et al. (1987) observe that many interacting galaxies can have enhancements in their H α fluxes and equivalent widths both near their centers and in their disks.

If interacting galaxies can undergo bursts of star formation, then it is necessary to study also the gas component in those galaxies. This has been done by several authors. Young et al. (1986 a,b), using the observed CO integrated intensity as a measure of the H₂ mass, point out that the interacting galaxies in their sample, as a whole, possess a higher ratio of infrared luminosity to molecular gas mass ($L_{\text{IR}}/M_{\text{H}_2}$) than noninteracting galaxies. They suggest that interacting galaxies have enhanced star formation efficiencies. Sanders et al. (1986) show that the most highly disturbed galaxies in their sample are the galaxies which have the highest ratios of far infrared luminosity to molecular gas mass. Using a larger data set,

Solomon and Sage (1988) find that the $L_{\text{IR}}/M_{\text{H}_2}$ ratios for interacting galaxies are significantly higher than those for non-interacting galaxies only if the morphological disturbances of the interacting galaxies are severe. They also find that galaxies which are believed to be in the process of merging have, on average, a lower $L_{\text{IR}}/M_{\text{H}_2}$ ratio than interacting galaxies which are not believed to be merging. It should be noted that the above mentioned results display a large amount of scatter, indicating that interacting and merging galaxies cover a wide range in their star formation properties.

Other less direct observations also bear out the idea that the gravitational interaction of two galaxies can lead to a burst of star formation in one or both of the galaxies. Fabbiano, Feigelson, and Zamorini (1982) find that the peculiar galaxies in their sample (many of which are interacting systems) have higher X-ray luminosities than galaxies without morphological peculiarities. They point out that their measurements can be explained by postulating a high formation rate of massive stars and hence a high supernova rate which gives rise to the X-ray flux. Rieke (1988) observed the hard X-ray (2-10 keV) fluxes of several ultraluminous infrared galaxies, some of which are merging systems. He finds that the hard X-ray fluxes arising from these galaxies are much weaker than those associated with the non-thermal continua observed in quasars and the nuclei of Seyfert galaxies. As one possibility to explain this observation, he suggests that the strong infrared luminosity is produced by a high rate of star formation.

If interacting galaxies are indeed undergoing bursts of star formation, then the gas out of which the stars form must first be

affected by the interaction. As a first step toward understanding why it is that interacting galaxies form stars more rapidly and more efficiently one must first examine the state of the interstellar medium during the interaction. The often quoted scenario is that as a result of the gravitational perturbation placed on a galaxy by the close passage of another, the gas clouds in that galaxy will acquire a larger velocity dispersion and hence will collide more frequently (e.g., Scalo and Struck-Marcell 1986). Noguchi and Ishibashi (1986), using a two dimensional model, show that the cloud-cloud collisional rate does indeed go up for the cases they consider. This model has several limitations. First, it is two dimensional while it is expected that the vast majority of interacting galaxies have their disks inclined to the orbital plane of the two galaxies. The substantial perturbation perpendicular to the gaseous disk may increase the disk scale height and reduce the cloud-cloud collisional rate. Noguchi and Ishibashi (1986) also assume that the gravitational potential of the galaxy remains fixed throughout their calculations, but this condition is relaxed in a later paper (Noguchi 1988). Second, Noguchi and Ishibashi (1986) do not address in detail the question of what happens to the clouds when they collide with one another. They assume that when two clouds collide they rebound off each other, dissipating roughly one half of their relative kinetic energy in the process. Cloud-cloud collisions, however, are expected to be more complicated. Depending on the masses of colliding clouds and their relative velocity, a collision can lead to coalescence or disruption of the colliding partners (Latanzio and Henriksen 1988). Thus the cloud mass spectrum evolves. Noguchi and Ishibashi (1986)

also assume that stars will form as a direct result of each collision, thereby equating the star formation rate just to the cloud-cloud collisional rate.

Here, before making an immediate link of a galaxy-galaxy interaction to a higher cloud-cloud collisional rate and an implied higher star formation rate, details of the evolution of the gas clouds during the gravitational interaction between two galaxies are followed. How the strength of the interaction affects the rate at which clouds coalesce versus the rate at which they disrupt shall be determined. The evolution of the cloud mass spectrum and of the cloud-cloud collisional velocity dispersion shall be examined. Then, combining these results with the observational evidence that interacting galaxies can form stars more readily and more efficiently than isolated galaxies, I hope to ascertain if the higher star formation rates are related to the frequency of cloud-cloud collisions, the degree of violence (as measured by the relative velocity) of the collisions, or, as is the case in a quiescent galaxy, to the buildup of massive clouds.

Accordingly a three dimensional model for gas clouds orbiting in the gravitational potential of a galaxy which at some later time is perturbed by the gravitational influence of another galaxy is developed. To do the problem correctly it is necessary to take into account the self-gravity of each galaxy since the redistribution of mass in the galaxy will itself act as a perturbation on the cloud system. To this end, the method of a multipole expansion of the gravitational field produced by a set of particles distributed in space to represent the disk and halo mass distributions of a galaxy

is used. This method was chosen for three reasons. First, as pointed out by White (1983), this method suppresses two-body relaxation effects which affect other N-body techniques (e.g. tree codes) and which would unrealistically increase the velocity dispersion of the gas clouds (see also White [1988] for a detailed discussion of some of the limitations of various N-body techniques). Secondly, the number of calculations scales linearly with the number of particles. Finally, this method will also enable us to study the merging of two galaxies, which can only be modelled when the gravitational field of each galaxy is calculated self-consistently. The merging phenomenon is interesting because a large fraction of interacting galaxies will eventually merge (Farouki and Shapiro 1982, Barnes 1988) and the galaxies with the highest observed infrared luminosities are also those which are believed to be merging. The method of multipole expansion has been employed by others for a wide variety of applications. McGlynn (1984) used it to study the dissipationless collapse of a set of gravitating particles while Fry and Peebles (1980) studied clustering in the universe. White (1983), Villumsen (1982), and Aguilar and White (1986) also used this method in the study of interacting and merging galaxies.

Chapter 2 describes the model in detail and chapter 3 summarizes the results of several experiments, which are designed to study the effects of the impact parameter of the galaxy-galaxy interaction. A theory for the relation between cloud-cloud collisions and star formation and interacting galaxies is also developed in chapter 3. The angle between the orbital angular momentum vector of the two galaxies and the spin angular momentum vector of one of the

galaxies which contains gas (inclination), bound and unbound orbits, the mass of the perturbing galaxy, and the effect of having gas in both galaxies in a case when the galaxies merge are considered in chapter 4. In the final chapter I summarize the important points.

CHAPTER 2

MODEL

2.1 Gravitational Field Calculation

The multipole expansion of an arbitrary distribution of matter is given by (Jackson 1975),

$$\Phi(\mathbf{r}, \mathbf{r}') = -4\pi G \sum_{\ell=0}^{\infty} \frac{1}{2^{\ell+1}} \sum_{m=-\ell}^{\ell} \left(\int Y_{\ell m}^*(\theta', \phi') \frac{r_{<}^{\ell}}{r_{>}^{\ell+1}} \rho(\mathbf{r}') d^3\mathbf{r}' \right) Y_{\ell m}(\theta, \phi)$$

where $\Phi(\mathbf{r}, \mathbf{r}')$ is the gravitational potential at \mathbf{r} due to a mass element located at \mathbf{r}' , $r_{<}$ and $r_{>}$ are the lesser and greater, respectively, between the radial coordinates r and r' , and $Y_{\ell m}$ are the spherical harmonic functions. For a system of point masses the density function $\rho(\mathbf{r}')$ can be replaced by $m_i \delta(\mathbf{r}-\mathbf{r}_i)$ where m_i is the mass of particle i . This allows us to define a set of coefficients:

$$B_{\ell m}^1(r) = \sum_{int} m_i Y_{\ell m}^*(\theta_i, \phi_i) \frac{r_i^{\ell}}{r^{\ell+1}} \quad ; \quad r_i < r$$

$$B_{\ell m}^2(r) = \sum_{ext} m_i Y_{\ell m}^*(\theta_i, \phi_i) \frac{r^{\ell}}{r_i^{\ell+1}} \quad ; \quad r_i > r$$

where the sums are carried out over particles interior and exterior to the radius r . The expression for the total potential at \mathbf{r} then becomes,

$$\Phi(\mathbf{r}) = -4\pi G \sum_{\ell=0}^{\infty} \frac{1}{2^{\ell+1}} \sum_{m=-\ell}^{\ell} \left(B_{\ell m}^1(r) + B_{\ell m}^2(r) \right) Y_{\ell m}(\theta, \phi) \quad .$$

The expressions for the acceleration in each direction are then

easily found through the application of $\mathbf{g} = -\nabla\Phi$, where \mathbf{g} is the acceleration vector. Villumsen (1982) points out that if r or r_i is small, two-body interactions become important near the center of coordinates. So, in the above expressions each r or r_i in the denominator is softened by an amount δ , i.e. $\sqrt{(r^2 + \delta^2)}$ is used in place of r . The softening parameter, δ , is given a value of 1 kpc. This is equal to that used by Villumsen (1982) and smaller than that used by White (1983). White (1983) shows that there is an instability in the position of the density center of the galaxy due to the truncation of the multipole expansion. To avoid this, I follow White (1983) and soften the terms with $\ell > 0$ by twice the amount used for the $\ell = 0$ terms. A core particle with 0.1 times the mass of the entire galaxy is placed at the center of the galaxy to also help stabilize the position of the density center. The center of coordinates is chosen to lie on the density center of the galaxy.

10^4 particles are used to simulate the disk and halo mass distributions of the galaxy. Half of them are distributed in a disk according to an exponential surface density law with a scale length of 4 kpc and a truncation radius of 10 kpc. The disk particles are given tangential velocities corresponding to circular orbits about the center of the galaxy; in addition, small random velocities are added according to Toomre's (1964) criterion to stabilize the disk against the growth of axisymmetric disturbances. The other half of the particles are distributed in a spherical volume with a r^{-2} radial density law which is truncated at 15 kpc. Each halo particle is given a velocity in a random direction of magnitude $\sqrt{GM_{\text{halo}}/15 \text{ kpc}}$ such that the halo is initially in rough virial equilibrium. At each

time step in the calculation the particles are first sorted according to radius. Next, the values of $B_{\ell m}^1$ and $B_{\ell m}^2$ are calculated on a radial grid which has a spacing of 0.1 kpc between grid points. The grid extends from $r = 0$ to $r = 50$ kpc. The values of $B_{\ell m}^1$ and $B_{\ell m}^2$ for each particle are found by interpolation between grid points. If a particle lies beyond 50 kpc, then the values of $B_{\ell m}^1$ and $B_{\ell m}^2$ used are

$$B_{\ell m}^1(r) = B_{\ell m}^1(50 \text{ kpc}) \left(\frac{50 \text{ kpc}}{r} \right)^{\ell+1}$$

$$B_{\ell m}^2(r) = 0.0 .$$

This method is similar to that employed by McGlynn (1984). In order to adequately model the acceleration perpendicular to the disk, the expansion above is carried out to $\ell = 10$. For an axisymmetric disk, the only nonzero terms are those with $m = 0$. Therefore, to save computing time, all m terms are kept for only $\ell \leq 4$. Beyond $\ell = 4$ only terms with $m = 0$ are kept. Following the logic of McGlynn (1984), the $m = 0$ terms are reduced for $\ell \leq 10$ by a factor $c_\ell = (1 - \frac{\ell}{11})^{0.25}$ in order to reduce the side lobes of the angular distribution caused by the truncation of the expansion at finite ℓ . It was found through experimentation that this factor best smoothed the functional form of the force perpendicular to the disk while maintaining the same magnitude as that in the full expansion. Terms with $m \neq 0$ and $\ell \leq 4$ are reduced by the factors given by McGlynn (1984).

The second galaxy is modelled in the same way as that described above, except that the center of coordinates is moved to the density center of this galaxy and the values of $B_{\ell m}^1$ and $B_{\ell m}^2$ due to this

second set of 10^4 particles representing the halo and disk mass distributions are calculated. Each galaxy is initially given a position and velocity such that their relative motion is parameterized by b , the impact parameter, and γ , the ratio of the relative kinetic energy of the two galaxies to their gravitational binding energy determined by treating them as mass points. If $\gamma = 1$ the orbits for two mass points would be parabolic. The angle of inclination, i , is the angle between the angular momentum vector of the orbit of the two galaxies and the spin angular momentum vector of the galaxy containing gas clouds. Hence if $i = 0^\circ$ the orbit is coplanar with the gaseous disk and prograde with respect to the spin of the galaxy.

2.2 Cloud-Cloud Collisions

The two galaxies are allowed to relax for a period of 300 million years (until the values of $B_{\ell m}^1$ and $B_{\ell m}^2$ vary by no more than a few percent) before the gas clouds are introduced into the system. At this time a number of particles, depending on the mass of gas chosen, which represent gas clouds are placed on circular orbits in the disk of one or both of the galaxies. From 4 to 8 kpc the clouds are distributed with a constant surface density. Inside 4 kpc they are distributed with an exponential surface density similar to that given to the disk stars and normalized to join smoothly with the cloud distribution beyond 4 kpc. Each cloud is also initially given an additional 7 km s^{-1} velocity in a random direction. Each cloud is assigned a mass according to a poisson distribution peaked at 5×10^4

M_{\odot} and normalized to the total mass of the cloud system. The two galaxies are placed far enough apart on their orbits to give the cloud system roughly 500 Myr to relax into an equilibrium configuration before perigalacticon.

As the clouds move in the time-dependent gravitational field of the two galaxies in orbit about each other they are allowed to collide. Collisions are searched for at each time step, which is 1 Myr. If two clouds lie within a distance smaller than the sum of their radii the clouds are said to have collided.

Latanzio and Henriksen (1988) perform numerical simulations which model two colliding clouds. They vary the relative velocity and the impact parameter of the collision along with the rotational rates and orientations of the two colliding clouds. They find that when two clouds collide with an impact parameter of $b = R$, where R is the radius of one of the clouds, the clouds coalesce if their parameter γ_c (the ratio of the relative translational kinetic energy measured in the center of mass reference frame to the total gravitational binding energy of the two-cloud system when the clouds are just in physical contact) is less than 1.25. They go on to suggest that a rough condition for the coalescence of two colliding clouds is $\gamma_c \leq 4$, but this condition strictly applies only to head-on collisions.

Most collisions between interstellar clouds will be off center and the criterion for coalescence or disruption which is adopted based upon the $b = R$ simulations of Latanzio and Henriksen (1988).

This condition is expressed in the following way: if

$$\frac{1}{2} \left(\frac{m_1 m_2}{m_1 + m_2} \right) v_{rel}^2 \leq \frac{G m_1 m_2}{r_{12}} + \frac{3}{5} \frac{G m_1^2}{R_1} + \frac{3}{5} \frac{G m_2^2}{R_2}$$

the clouds are said to have coalesced. The parameters m_1 and m_2 are the masses of the two clouds, R_1 and R_2 are their radii, r_{12} is the distance between their centers, and v_{rel} is their relative velocity. A new cloud of mass $(m_1 + m_2)$ is placed at the center of mass of the two original clouds. It is given a velocity such that the momentum of the original clouds is conserved. If the above condition is not satisfied, then the clouds are said to break up and this is counted as one collisional disruption. The mass of the region of each cloud which overlaps with the other cloud is computed. Each is subtracted from the mass of the original cloud. The velocities of these two remainders are not altered. A third cloud which has a mass equal to the sum of the masses of the two overlap regions is created and given a position at the center of mass of the two original clouds and a velocity such that the momentum of the overlap regions is conserved. If the total overlap mass is less than $10^4 M_\odot$ the collision is counted but a new cloud is not created in this case to prevent the buildup of a large number of small clouds. A collision of this type is referred to as a glancing collision and that which produces a third cloud of mass $\geq 10^4 M_\odot$ as a large collisional disruption.

A different criterion for cloud coalescence than the one stated above has also been considered. This was considered because if the masses of the two colliding clouds are very different, i.e. $m_1 \gg m_2$, the condition for coalescence in the expression above becomes $\frac{1}{2} m_2 v_{rel}^2 < \frac{3}{5} G m_1^2 / R_1$. This condition implies that the internal gravitational

binding energy of the larger cloud dominates and that the kinetic energy is completely equilibrated with the larger cloud, which is probably not the case. Therefore, we could overestimate the rate at which clouds coalesce. In this second criterion it is assumed that the kinetic energy is dissipated only in the overlapping regions of the colliding clouds. The overlapping regions are assumed to form a third cloud with a velocity which is determined from momentum conservation. Next, the relative kinetic energy (T_{rel}) of this third cloud is compared with the gravitational binding energy between it and the non-overlapping portion of the larger cloud (Ω), assuming a separation equal to the larger cloud's radius. If $\Omega > T_{rel}$ the non-overlapping portion of the larger cloud and the third cloud are assumed to coalesce, otherwise the collision is counted as a large collisional disruption. If $\Omega > T_{rel}$ the relative kinetic energy of the non-overlapping portion of the smaller cloud will also be compared with the gravitational binding energy between it and the coalesced cloud to determine if it too can become absorbed. Using this second criterion in a few computer runs, it was found that the coalescence rate and the rate of build up of massive clouds are lowered. However, the changes are not large and, for simplicity, we have adopted the first criterion for all the cases considered here.

Each cloud is assumed to have a uniform density so that the cross sectional area of a cloud depends on its mass in the following way (Kwan and Valdes 1987),

$$\sigma(m) = 625 \left(\frac{m}{10^5 M_{\odot}} \right)^{2/3} \text{ pc}^2 .$$

In our own galaxy most of the cloud-cloud collisions lead to cloud coalescences and mass growth, while the formation of massive stars is observed to be predominantly associated with the most massive clouds. To allow for the breakup of a cloud due to star formation, I follow Kwan and Valdes (1987) in stipulating that once a cloud grows to $10^6 M_{\odot}$ it breaks up due to star formation in its interior on a time scale given by,

$$t(m) = \frac{70 \text{ Myr}}{1 + \log \left(\frac{m}{10^6 M_{\odot}} \right)} .$$

In their study Kwan and Valdes (1987) also varied the value of the numerator. They found that the mass spectrum of clouds does not depend sensitively on this parameter so it is not varied in this study. When a cloud breaks up in this way, the mass of the original cloud is divided up into a number of small fragments which are each given, in addition to the original velocity, a 7 km s^{-1} velocity away from the center of the original cloud. The mass of each fragment is determined by sampling a poisson distribution peaked at $5 \times 10^4 M_{\odot}$. No fragment is allowed to have a mass greater than $2 \times 10^5 M_{\odot}$.

The method of multipole expansion described above was chosen primarily because it effectively suppresses two-body encounters which are present in other N-body calculations (e.g., tree-codes [Barnes and Hut 1986]). We are, for the most part, interested in finding out if the interaction of two galaxies leads to cloud-cloud collisions which are predominantly coalescing or disruptive. In a quiescent galaxy most cloud-cloud collisions occur at low relative velocities, leading to coalescence and mass growth. Therefore, a method for

calculating the gravitational field which does not artificially inflate the velocity dispersion of the clouds is necessary. If two-body scatterings between gas clouds and "stars" are large (as is the case with tree codes) we would bias our result towards collisional disruption of clouds even before the perturbation of a second galaxy is introduced. For a discussion of some of these considerations see White (1988) and Sellwood (1987). The method of multipole expansion does lack some of the resolution attained by other codes but it is adequate for the purpose at hand.

The code has been tested in the following manner. First, it conserves energy to within 1% over the time of a simulation. Secondly, it reproduces the time scales for merging and the density distributions of the merger remnants found by Farouki and Shapiro (1982) who modelled the merging of two disk galaxies using direct summation to calculate the force on each particle. As a further test, Noguchi's (1988) result that a strong bar can form as a result of the interaction of two galaxies (provided the rotation curve of the galaxy is rising out to 25% - 50% of the disk radius and is flat thereafter) was considered. Adjusting the mass distribution to give such a rotation curve, the multipole expansion code also produces a strong, long-lived bar.

To test the introduction of gas clouds into the multipole expansion code and to obtain a fiducial value of the cloud-cloud collision rate, the evolution of the cloud system in a quiescent galaxy was first examined. Two cases were calculated, one where the potential of the galaxy was held fixed and another where the potential was computed in the manner described above. In both cases

the collisional rate declines near the beginning of the calculation, owing to a diminishing number of clouds as they coalesce. When enough massive clouds are built up so that the rate at which these clouds are disrupted due to star formation increases, the collisional rate rises. It reaches an equilibrium value after roughly 400 Myr and remains stable thereafter. The main difference between the two cases is that the total collisional rate in the case where the gravitational potential is calculated using the multipole expansion is roughly a factor of 1.5 higher than that in the case where the potential is held fixed. In both cases the great majority of collisions lead to coalescence. This comparison of the two calculations gives some confidence that the behavior of the cloud system in the case where the gravitational potential is calculated using the multipole expansion code is quantitatively not too far off. To test the code when the perturbation of another galaxy is present a restricted three-body code was constructed in which the clouds orbit in a constant gravitational potential and are, at some later time, perturbed by another identical potential. The galaxy orbits were chosen such that the galaxies would not merge. When the same case was run using the multipole expansion code, the results, in terms of the total number of collisions induced by the interaction, the number of coalescing collisions, and the number of large disruptive and glancing collisions, were the same to within a small factor. When the perturbation due to the close passage of another galaxy is added we are interested in the behavior of the cloud system relative to that in the unperturbed state. The changes, as shall be seen, are very dramatic.

CHAPTER 3

VARIATIONS WITH IMPACT PARAMETER

3.1 Results

In this chapter I shall describe a small set of three simulations of the interaction of two galaxies. Since the tidal force depends most strongly on the distance separating the two galaxies only the impact parameter, b , is varied for this study. The inclination of the galaxy which contains gas clouds to the orbital plane is set at 30° and γ is set equal to 1. The three cases considered are $b = 60$ kpc, $b = 40$ kpc and $b = 20$ kpc, respectively.

3.1.1 $b = 60$ kpc

The first case considered has an impact parameter of 60 kpc. This places the galaxies on orbits which bring them to within a distance of 30.6 kpc at a time of closest approach of 904 Myr after the start of the calculation. The morphology of the cloud system is not highly disturbed in this case (Fig. 1). Near closest approach the galaxy takes on a slightly oval shape. At 1200 Myr, which is 300 Myr after the time of closest approach, prominent spiral arms appear which persist until 1400 Myr but appear only faintly by the end of the calculation at 1700 Myr. No tails or bridges form at any time.

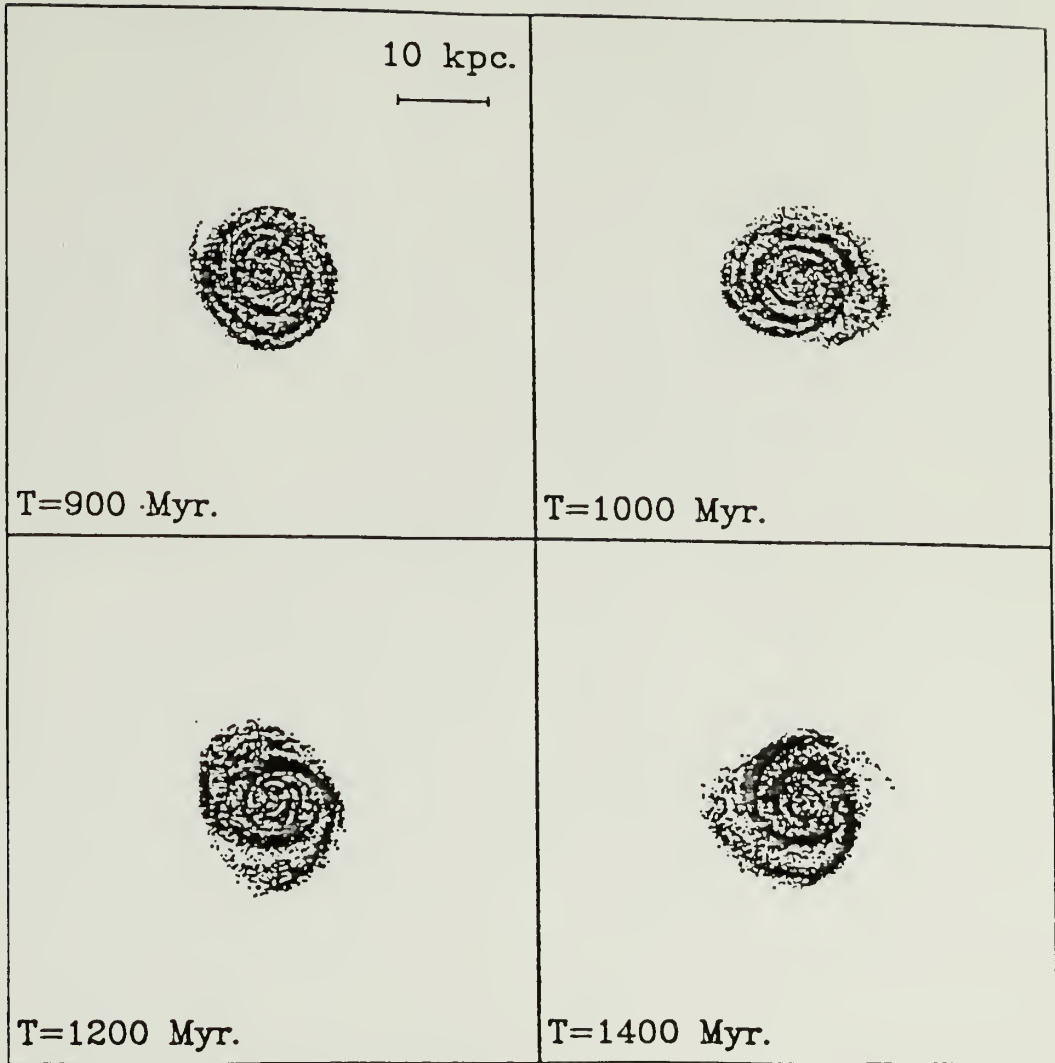


Figure 1 The morphological change of the cloud system for case 1. Closest approach occurs at 904 Myr and the distance of closest approach is 30.6 kpc. All views are face-on in the rest frame of the galaxy.

To examine the response of the cloud system to the galaxy-galaxy interaction as a function of position, shown in Figures 2 and 3 is the behavior of the cloud system in regions beyond and within 2 kpc of the galactic center respectively. In each figure is shown the total rate of cloud-cloud collisions (which include coalescing, glancing, and large disruptive collisions), the rate of cloud coalescence, the rate of large collisional disruptions, and the rate of production of fragments from the disruption of massive clouds owing to internal star formation. As mentioned in chapter 2, the two galaxies are allowed to relax for a period of 300 Myr (so that the coefficients of multipole expansion reach steady state values) before the clouds are introduced in one of the galaxies, hence the beginning of the plots at a time of 300 Myr. It then takes ~ 400 Myr, or until a time of 700 Myr after the start of the calculation, for the cloud system to reach an equilibrium collision rate, which represents the unperturbed value.

For the region $r > 2$ kpc we see from Figure 2 no increase in the total rate of collisions until a time of 1000 Myr, or roughly 100 Myr after the time of closest approach. At its peak the total collision rate is raised to a factor of ~ 2.5 above the unperturbed value. Before the time of closest approach coalescences represent roughly 70% of all collisions. The coalescence rate, however, rises only slowly in response to the galaxy-galaxy interaction. Its peak value is higher than the unperturbed value by only $\sim 30\%$. At the time of the peak collisional rate after the time of closest approach coalescences represent only $\sim 40\%$ of all collisions. This indicates that the collisions which are induced by the interaction of the two

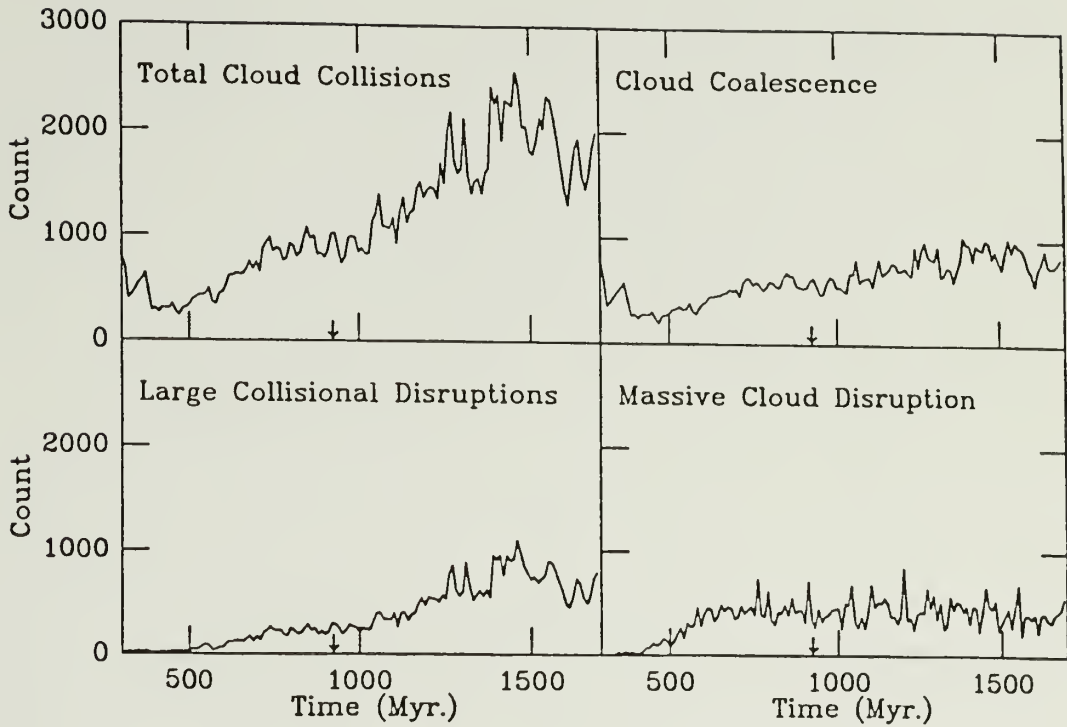


Figure 2 Time dependences, in the region exterior to 2 kpc of the galactic center, of the total rate of cloud-cloud collision (in units of number per 10 Myr), the rate of coalescence, the rate of large collisional disruptions, and the rate at which fragments are produced due to star formation in massive clouds. The total collisional rate comprises the rate of coalescence, the rate of large collisional disruptions and the rate of glancing collisions. The arrow marks the time of closest approach of the two interacting galaxies.

galaxies are of large enough energy that the majority of collisions disrupt the clouds. This is reflected in a substantial increase in the rate of large collisional disruptions which is raised by a factor of ~ 3 above its unperturbed value. Inside 2 kpc (c.f. Fig. 3), on the other hand, no significant departures from the pre-encounter values for any of the rates are noted.

The distribution of collisional velocities exterior to 2 kpc is broadened somewhat as a result of the interaction. Inside 2 kpc the change in the distribution of collisional velocities is small (see Fig. 4). No discernible changes are noted in the mass spectrum of clouds, either outside or inside 2 kpc.

3.1.2 $b = 40$ kpc

The second case considered here is one with an impact parameter of 40 kpc. In this case the galaxies do not merge but come to within 13.8 kpc of each other at perigalacticon which occurs at a time of 806 Myr after the start of the calculation. The morphological change in the gas cloud system as a result of the interaction is quite dramatic (Fig. 5). Shortly after closest approach prominent bridges and tails appear and remain apparent for a period of 400 Myr after closest approach.

The total rate of cloud-cloud collisions both within 2 kpc and exterior to 2 kpc increases dramatically a short time after closest approach (Figs. 6 and 7). Outside 2 kpc the total rate at its peak is elevated by roughly a factor of 13 above the pre-encounter value. Afterwards the collisional rate begins to fall and levels off at a

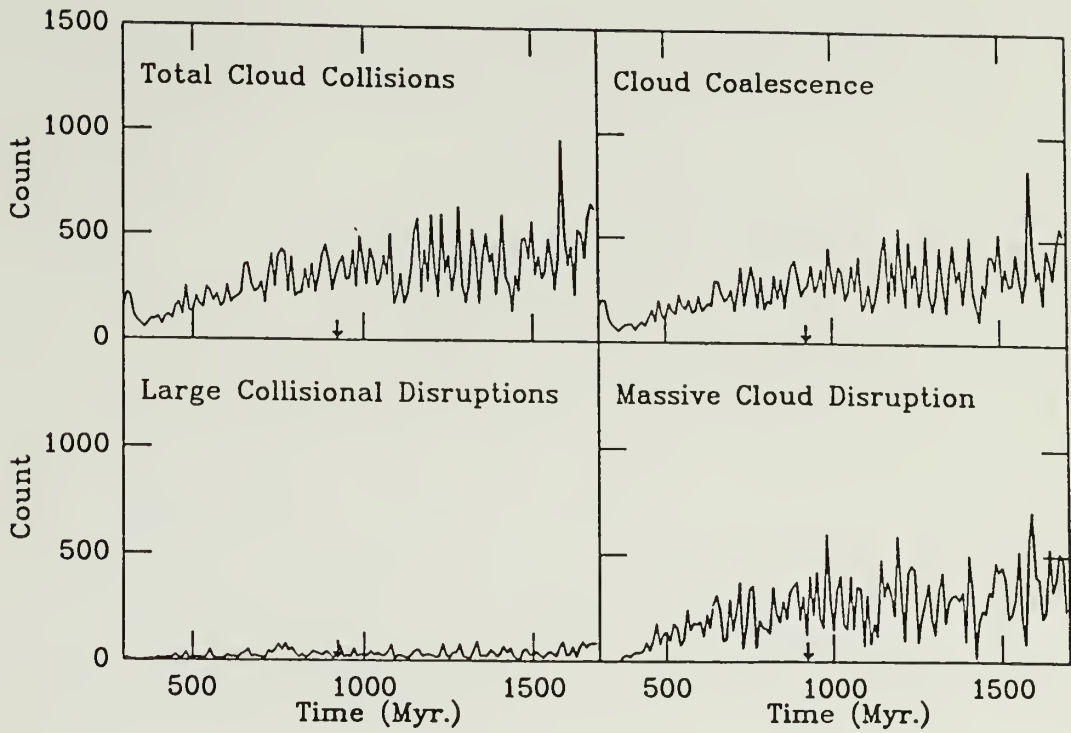


Figure 3 Same as Fig. 2 except for the region interior to 2 kpc.

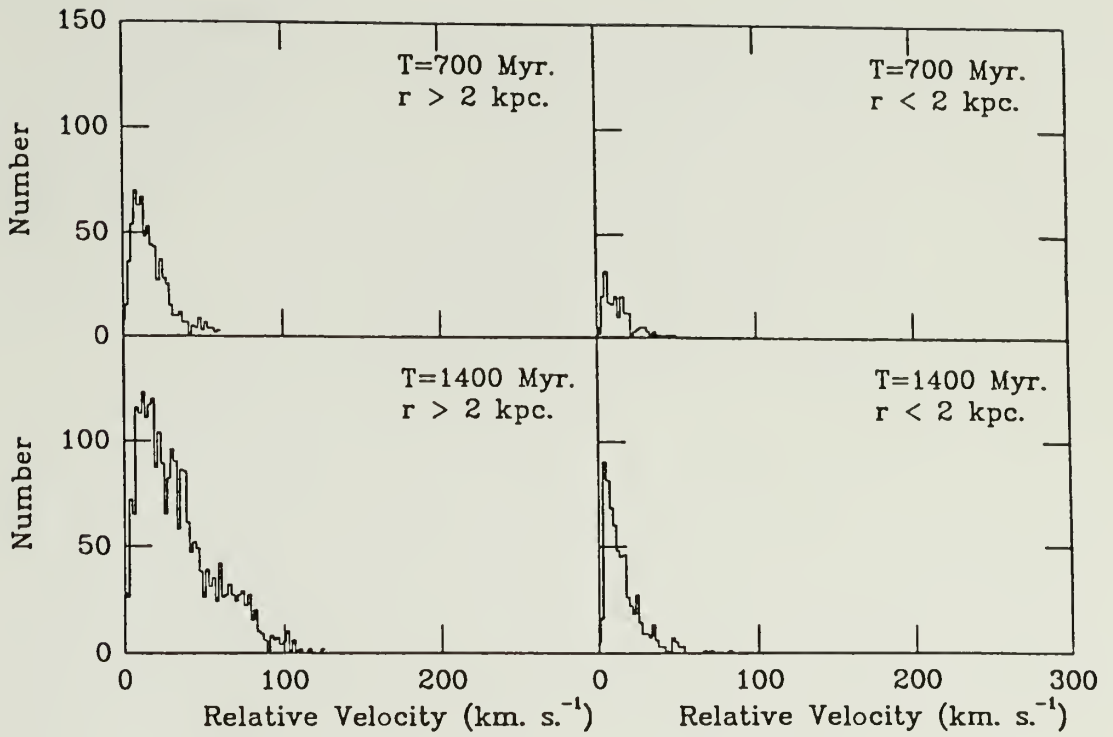


Figure 4 The distribution of collisional velocities before the time of closest approach and at the time of peak total collisional rate after closest approach.

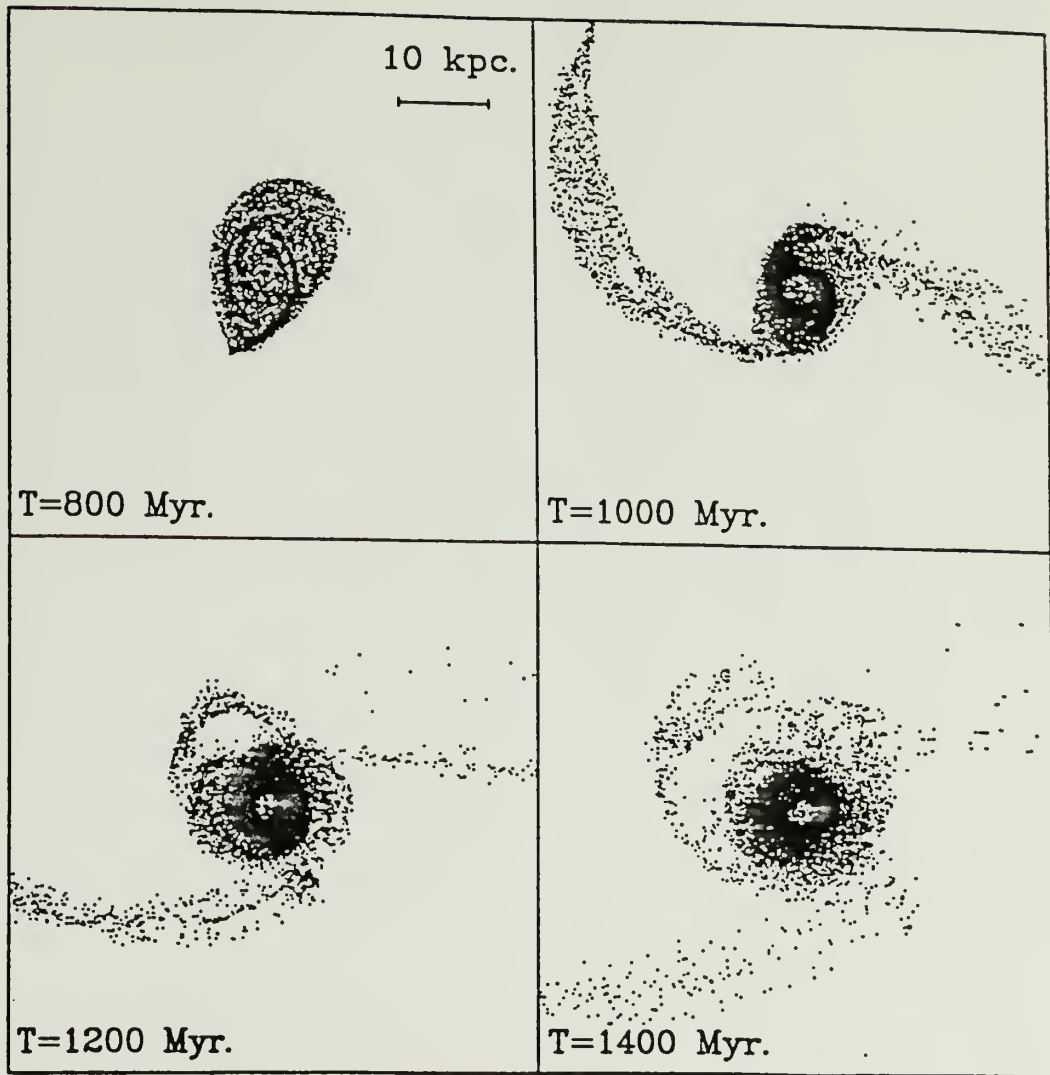


Figure 5 Same as Fig. 1 except for case 2. Closest approach occurs at a time of 806 Myr when the galaxies are separated by a distance of 13.8 kpc.

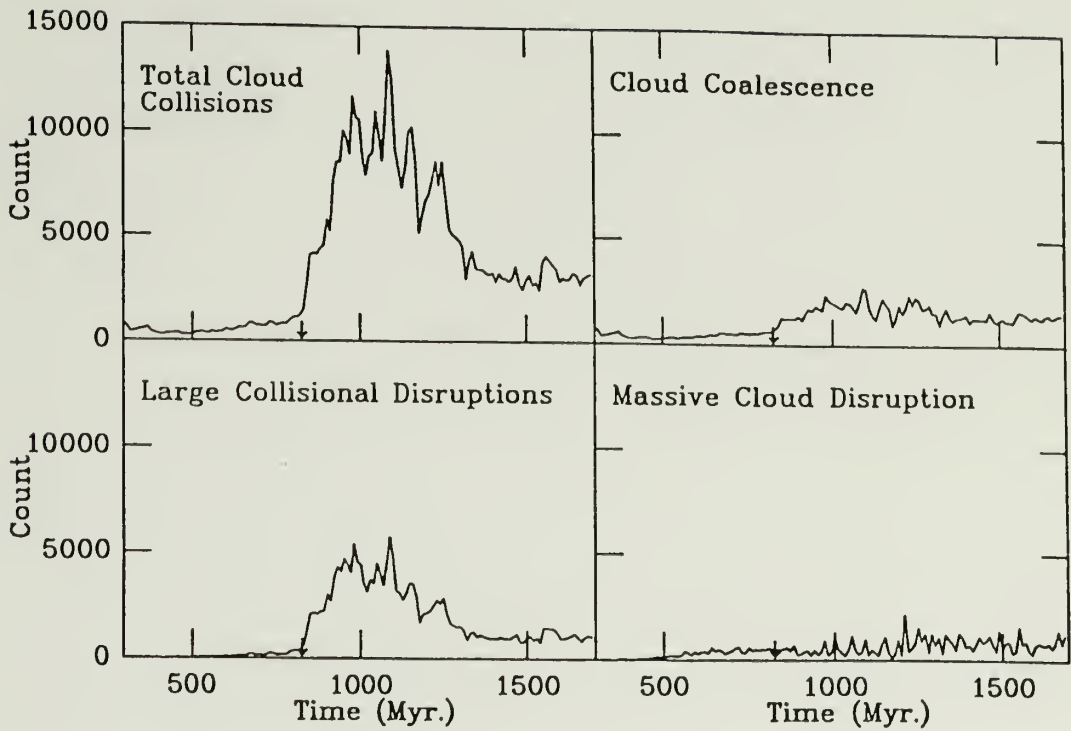


Figure 6 Same as Fig. 2 except for case 2, i.e. the region exterior to 2 kpc.

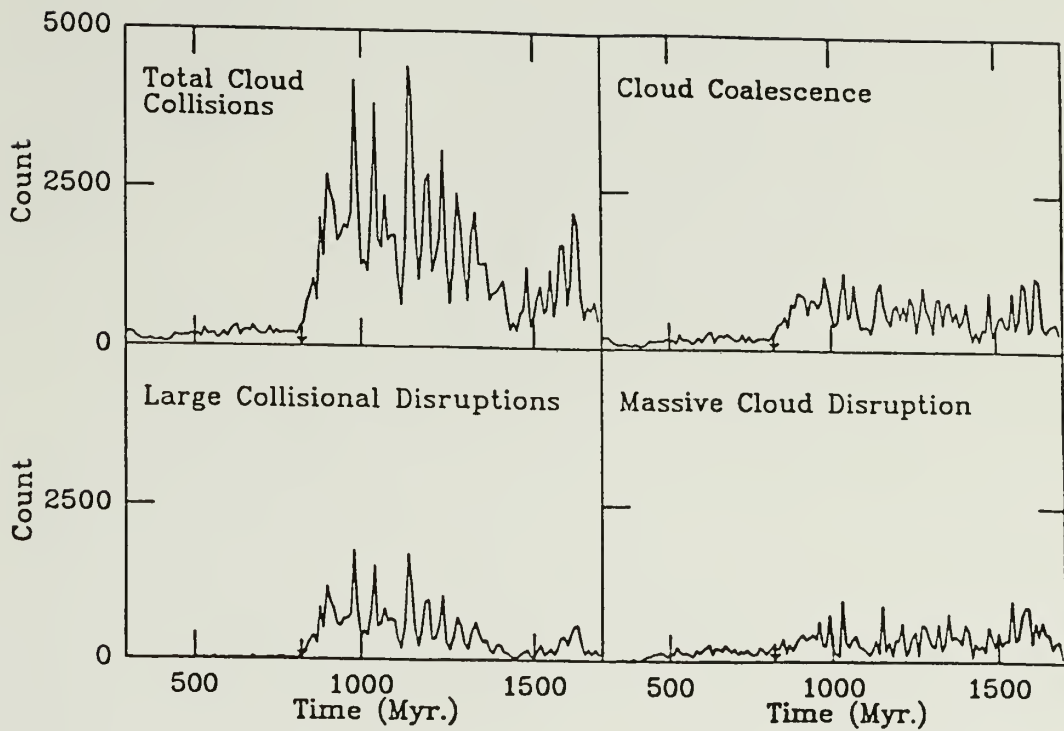


Figure 7 Same as Fig. 3 except for case 2, i.e. the region interior to 2 kpc.

value roughly 4 times higher than the pre-encounter rate. Inside 2 kpc the total rate of collisions is likewise increased, but by only a factor of ~ 8 over its unperturbed value. The rate at which clouds coalesce is also increased both in the central and outer regions of the galaxy. Its rise, however, is less dramatic. Indeed, the vast majority of collisions which occur after the closest approach of the two galaxies are either glancing collisions or large disruptive ones. Shortly after closest approach the rate of large collisional disruptions is raised by a factor of ~ 18 exterior to 2 kpc and by a factor of ~ 30 interior to 2 kpc. In both regions interior and exterior to 2 kpc only $\sim 20\%$ of all collisions are coalescences when the total collisional rate is at its peak. When this rate levels off after 1300 Myr coalescing collisions become relatively more frequent and they represent roughly one half of all the collisions. Looking at the rate at which new clouds are produced due to star formation in massive clouds, only a slight increase from the unperturbed value is noted. This indicates that even though the coalescence rate is increased and a slight increase in the number of clouds more massive than $10^6 M_{\odot}$ is noted, disruptive collisions are frequent enough to prevent the build up of a large number of very massive clouds.

The distributions of collisional velocities (Fig. 8) show that while the number of collisions is increased the dispersion in the distribution of collisional velocities is likewise increased. Before the interaction most collisions occur at velocities less than 10 km s^{-1} . After the close passage of the two galaxies the spread in the distribution is $\sim 60 \text{ km s}^{-1}$ with maximum velocities near 200 km s^{-1} . As the cloud system evolves after the interaction the

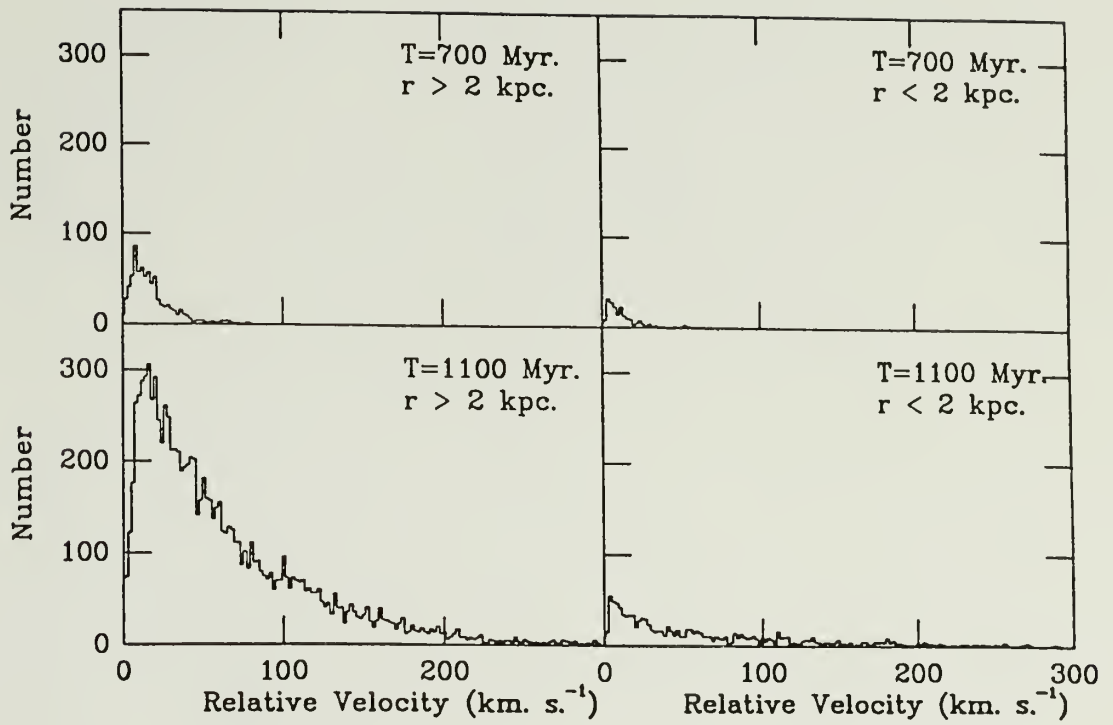


Figure 8 Same as Fig. 4 except for case 2.

cloud-cloud collisions dissipate a large part of the kinetic energy that was injected into the system by the close passage of the second galaxy, and the distribution of collisional velocities becomes less broad with time. Dissipation of energy is also evident in that the rate of coalescence represents a larger fraction of the total rate at the end of the calculation than at the time of the collision peak.

Comparing this case with the first one, it is found that not only is the collisional rate dramatically higher, but also the activity shifts toward the central region of the galaxy. This latter point is demonstrated more clearly in Figure 9 where plots of $2\pi r\sigma$ vs. r are shown at different times. Here σ is the surface density of the gas in the disk of the galaxy and r is the radius from the center. The plots show a strong evolution in the radial distribution of the gas. A fraction of the gas moves to larger radii ($r > 10$ kpc) as a result of the interaction, and an enhancement in the surface density of gas between 2 and 4 kpc appears soon after closest approach. From this it is evident that the majority of cloud-cloud collisions which occur exterior to 2 kpc are actually confined to the region between 2 and 4 kpc. Since the rate of collisions interior to 2 kpc is also greatly increased, it is clear that virtually all of the activity (i.e. increased rates of collision) induced by the interaction of the galaxies is confined to a region within 4 kpc.

3.1.3 $b = 20$ kpc

The last case considered is one with $b = 20$ kpc. In this case the galaxies merge within 300 Myr of their initial close approach

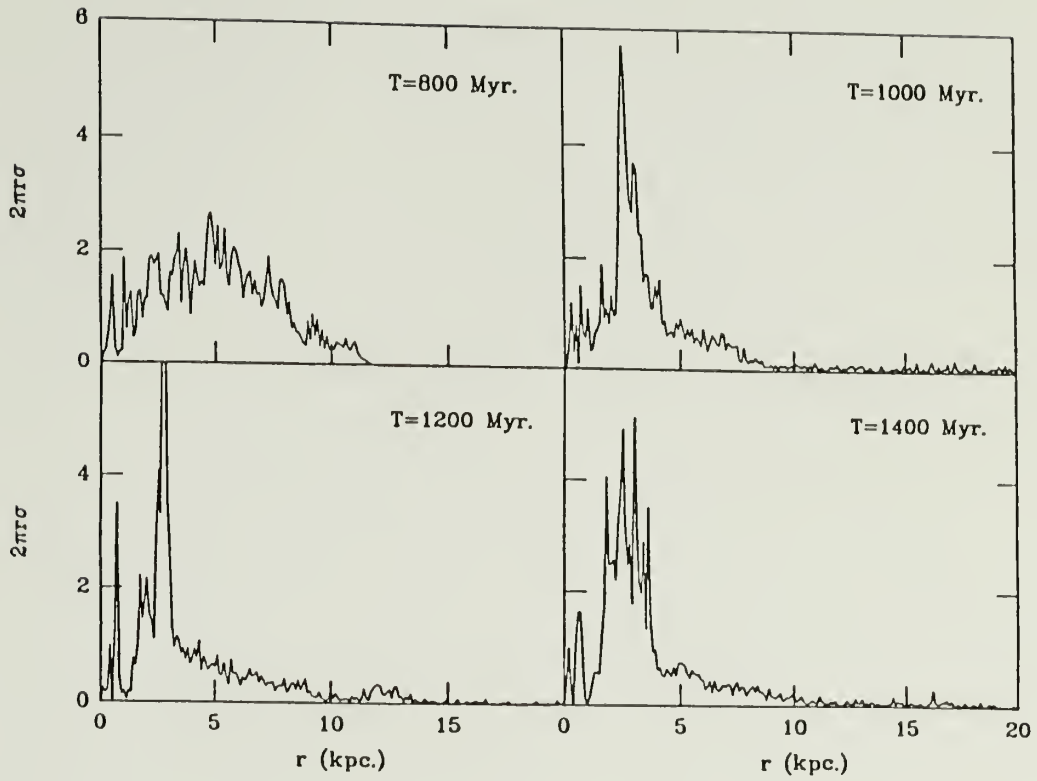


Figure 9 Plots of $2\pi r\sigma$ vs. radius at different times in case 2.

which occurs at 720 Myr. The morphological changes in this case are by far the most dramatic of the three cases considered so far (Figs. 10 and 11). Tails appear near the initial close passage of the galaxies but become diffuse rather rapidly and are no longer evident roughly 300 Myr after their first appearance. By this time the galaxies have merged and appear as a single elliptical-like object. Pictures of the cloud system show that large motions perpendicular to the disk of the galaxy are induced by the merger. Indeed, no disk is evident after the galaxies have merged.

The disruption of the disk is undoubtedly the reason why the rate of collisions exterior to 2 kpc is not elevated significantly by the merger, i.e. even though the clouds have a larger velocity dispersion they also occupy a larger volume of space. As seen from Figure 12 the total rate of collisions exhibits a sharp increase near the time of closest approach of the two galaxies, but then falls just as rapidly back to its pre-encounter value. The rate inside 2 kpc (Fig. 13), on the other hand, increases dramatically and remains elevated by a factor of ~ 20 up to the end of the calculation. The coalescence rate in the outer part of the galaxy actually drops to near zero after the close passage of the two galaxies so that all of the collisions which occur there are either glancing collisions or large disruptive ones. Interior to 2 kpc only ten percent of the collisions are coalescences after the time of closest approach so that large disruptive and glancing collisions represent an even larger fraction of the total than they do in the previous two cases. The rate of large collisional disruption interior to 2 kpc is raised above the unperturbed value by a factor of ~ 80 . Once again no

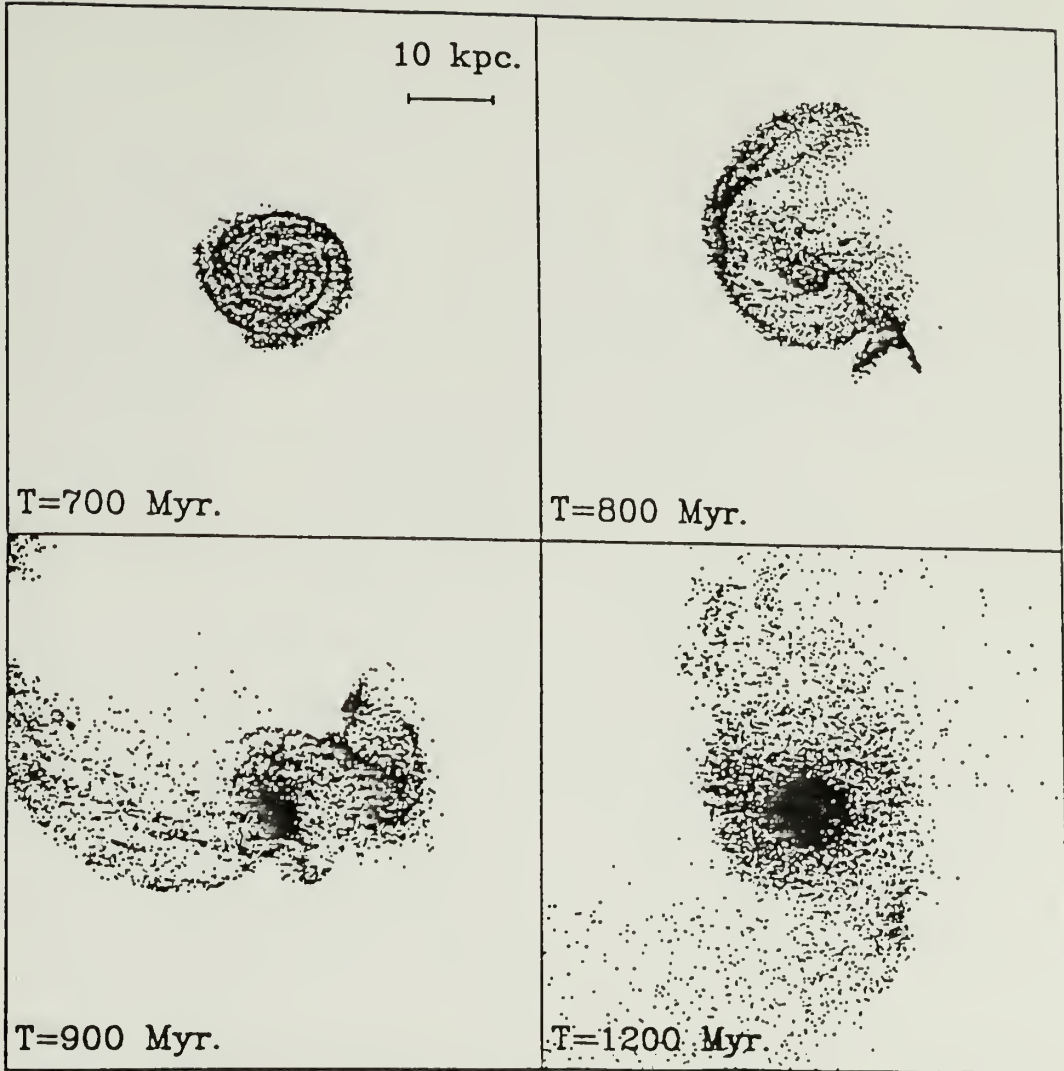


Figure 10 Face-on view of the morphological change of the cloud system in case 3 where the galaxies merge.

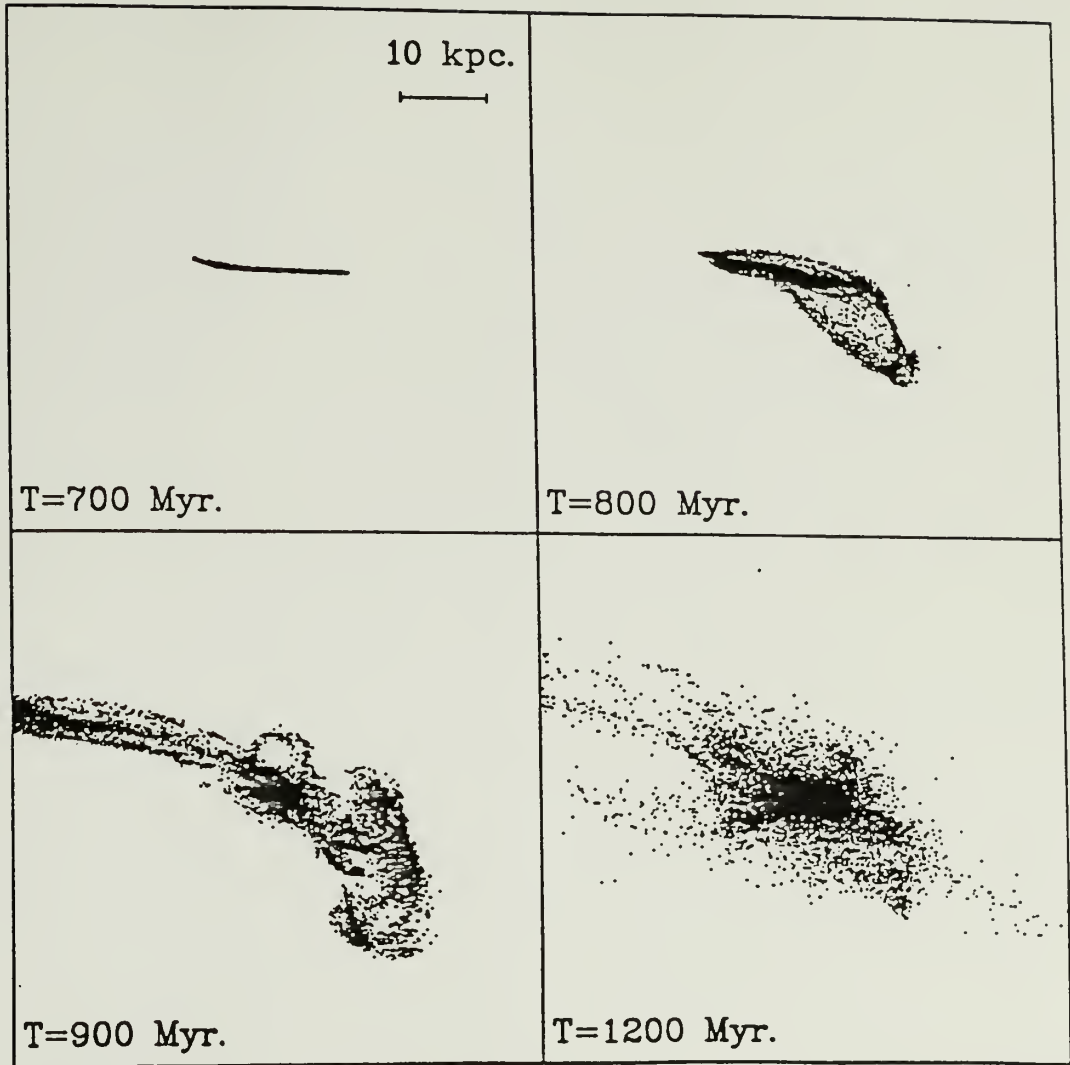


Figure 11 Edge-on view of the cloud system for case 3 showing the large motions induced perpendicular to the original disk of the galaxy.

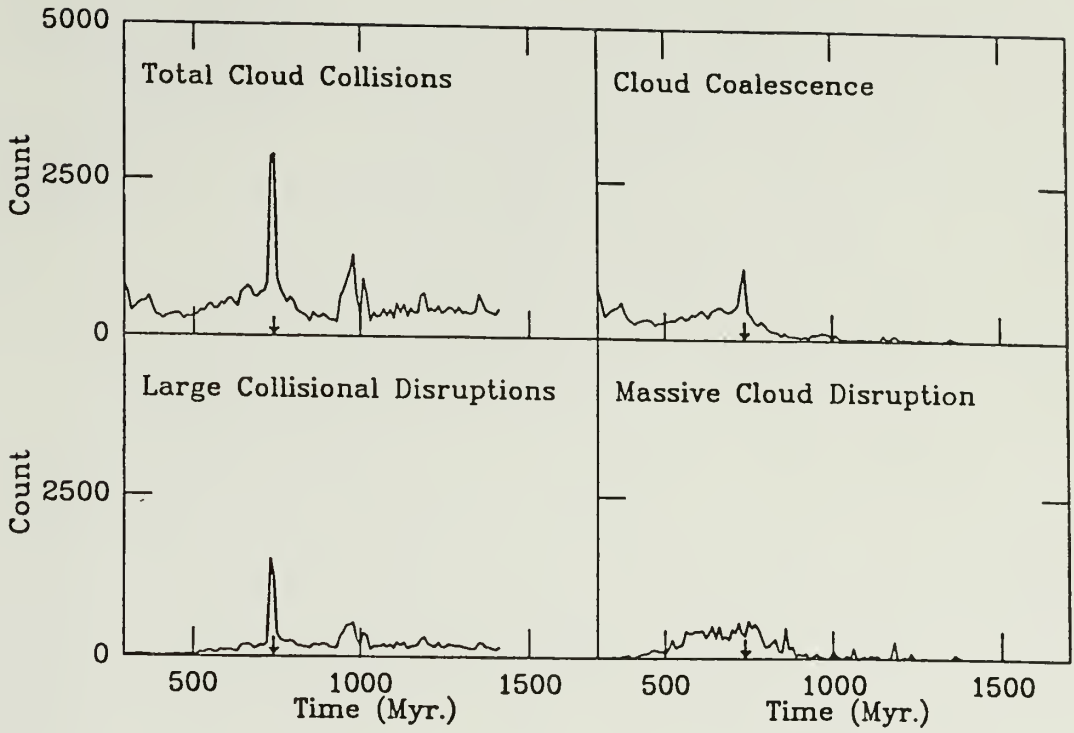


Figure 12 Same as Fig. 2 except for case 3, i.e. the region exterior to 2 kpc.

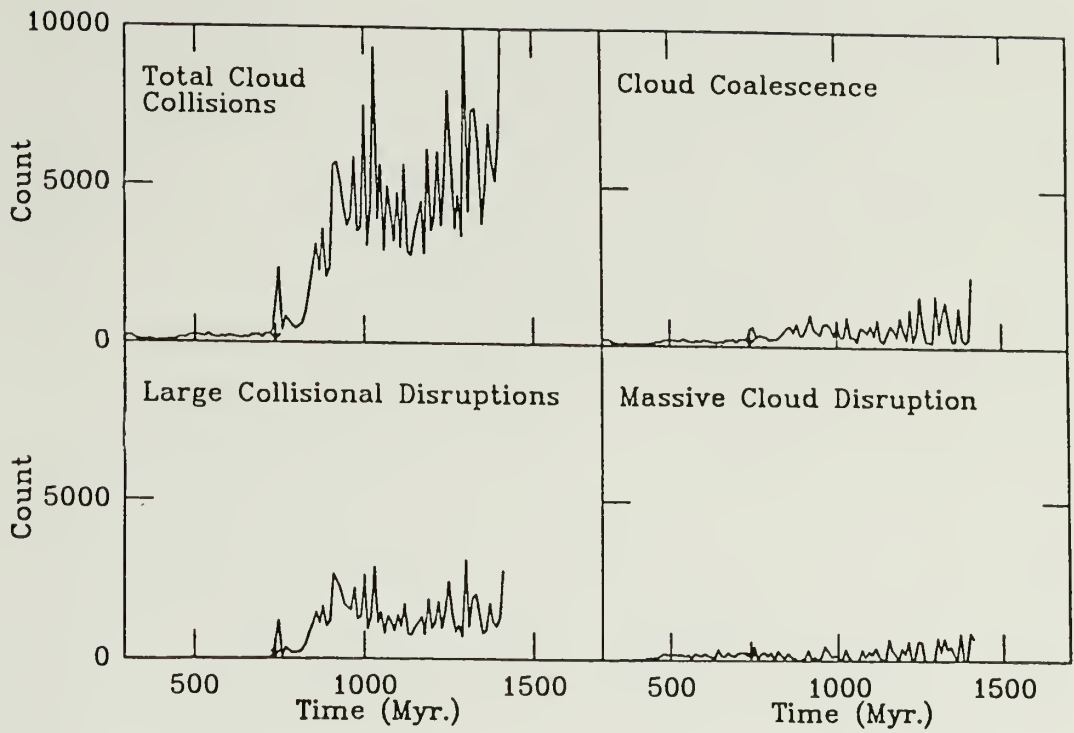


Figure 13 Same as Fig. 3 except for case 3, i.e. the region interior to 2 kpc.

increase in the rate at which fragments are produced due to the disruption of massive clouds by star formation is seen in either the interior or exterior of the galaxy.

The distribution of the velocities of collision as a result of the merger of the two galaxies becomes very much broader than that in the previous two cases. Here collisional velocities extend to beyond 300 km s^{-1} (Fig. 14). Also, unlike the previous two cases, no narrowing of this distribution is seen. Mass spectra are characterized by the production of a large number of small mass clouds.

Plots of $2\pi r\sigma$ vs. r (Fig. 15) show that a large fraction of the gas clouds move to larger radii. A peak in $2\pi r\sigma$ appears near the center of the galaxy and grows as the calculation proceeds. In this case it is clear that all the activity induced by the merger of the galaxies occurs very close to the center of the galaxy.

3.2 Discussion

From this limited set of experiments several results are already apparent. As the strength of the interaction between two galaxies becomes larger or, in the cases considered here, the closer the galaxies come to each other, the region in which the most activity is produced becomes increasingly concentrated toward the center of that galaxy. Secondly, the stronger the interaction, the smaller is the fraction of coalescing collisions. Correspondingly, the large collisional disruptions and glancing collisions comprise a progressively larger fraction of the total number of collisions after

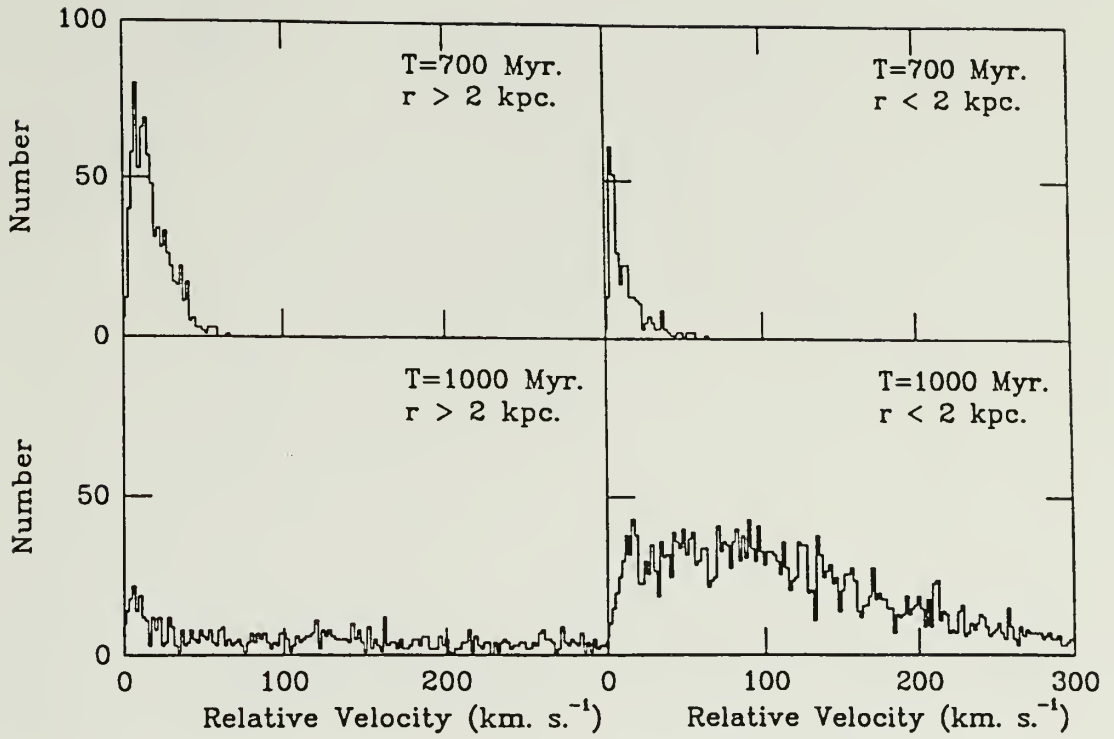


Figure 14 Same as Fig. 4 except for case 3.

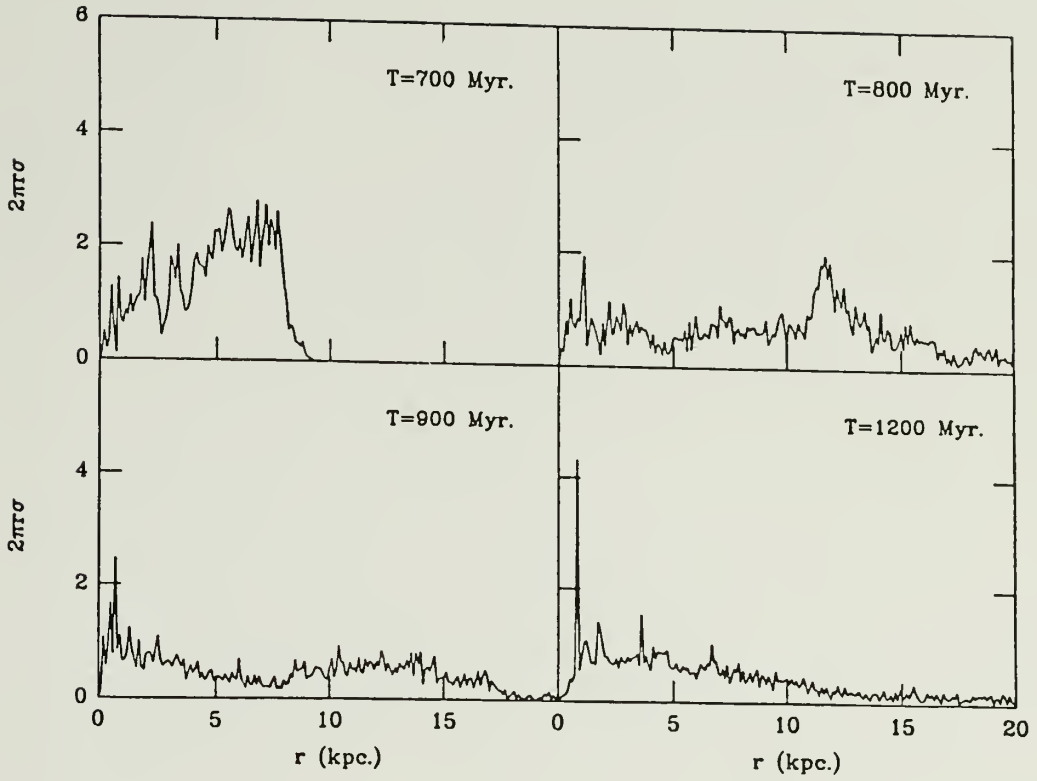


Figure 15 Same as Fig. 9 except for case 3.

the time of closest approach as the strength of the interaction increases. This is especially true interior to 2 kpc where the large collisional disruption rate does not increase from the unperturbed value in case 1, but increases by factors of ~ 30 and ~ 80 in cases 2 and 3 respectively. In other words, the stronger the interaction, the more disturbed and fragmented the interstellar medium becomes. Also, the stronger the interaction, the larger is the range of velocities with which the clouds collide. Lastly, there is no large increase above the unperturbed value in the rate of build up of massive clouds (indicated by the rate of production of fragments due to star formation) as a result of an interaction.

3.2.1 Cloud-Cloud Collisions and Star Formation

Observational evidence seems to indicate that interacting galaxies, on average, have higher star formation rates and star formation efficiencies when compared with noninteracting galaxies (e.g., Young et al. 1986a,b). The question then is: how do these models relate to any observed increase in star formation activity in interacting or merging galaxies? In case 1 (impact parameter of 60 kpc, $\gamma = 1$, and $i = 30^\circ$) the rates of cloud coalescence and production of fragments due to star formation in massive clouds remain unaffected, while the rate of large collisional disruption rises by a factor of ~ 3 after closest approach but does not exceed the cloud coalescence rate. I conclude that the galaxy-galaxy interaction is not strong enough to trigger an obvious burst of star formation in this case. Case 2 (impact parameter of 40 kpc, $\gamma = 1$,

and $i = 30^\circ$) is characterized by a much larger increase in the total rate of collisions after closest approach. The rate of cloud coalescence is raised above its unperturbed value by a factor of 3 while the rate at which fragments are produced due to star formation in massive clouds is raised by a factor of 1.5 to 2. Now the latter rate is roughly proportional to the rate of star formation in massive clouds. If the mechanism of star formation during an interaction is largely the same as it is in a quiescent galaxy, then case 2 would show only an increase of a factor of 1.5 to 2 in its star formation activity as a result of the interaction. If the burst of star formation which occurs is much stronger, one is led to conclude that a large portion of the star formation which is induced by the interaction is related to the cloud-cloud collisions which disrupt the clouds, since the disruptive collisions are elevated the most relative to their pre-encounter values and they represent the majority of the induced cloud-cloud collisions. Case 3 (impact parameter of 20 kpc, $\gamma = 1$, and $i = 30^\circ$) shows a more extreme difference between coalescing and disruptive collisions. Here, for the galaxy as a whole, the rates of cloud coalescence and the production of fragments due to star formation in massive clouds remain roughly unchanged or decrease slightly, while the rate of disruptive collisions (glancing and large disruptive) rises dramatically above its unperturbed value. If the burst of star formation occurs within ~ 700 Myr after the initial close approach, one is led to the same conclusion as that in the previous case. There is, however, the additional possibility in this case that as the cloud-cloud collisions dissipate the kinetic energy of the

clouds, a substantial amount of gas will sink toward the center of the merger remnant, the coalescence rate may then increase, and a burst of star formation may arise from an increase in the number of massive clouds. The time for this to occur, however, must be later than 700 Myr after the initial close approach of the two galaxies since no significant decrease in the collisional velocities by the end of the calculation is seen.

If stars form as a result of large disruptive and glancing cloud-cloud collisions the star formation rate and the associated luminosity produced as a result of the increased rate of disruptive collisions can be estimated. It is reasonable to assume that any star formation which is stimulated to occur when two gas clouds collide and disrupt will be confined to the regions of those clouds which are in physical contact with each other. Noguchi and Ishibashi (1986) make the assumption that when two clouds collide stars will form as a result. They do not consider, however, how much of the mass of the clouds will be converted to stars.

Even assuming that the overlap regions in disruptive collisions are the sites of star formation, another parameter must be specified in order to determine the star formation rate, \dot{M}_* . This is the fraction of the overlap mass that goes into stars, or the efficiency of star formation. Thus $\dot{M}_* = \epsilon \dot{M}_{\text{ovlp}}$. Case 2 was rerun for different values of ϵ . In the first run ϵ is set to 0, and \dot{M}_{ovlp} is determined as a function of time. This illustrates one extreme situation in which the star formation efficiency is so low that both the amount and dynamics of the gas clouds are unaffected by star formation. In the second run $\epsilon = 100\%$. This illustrates the

opposite extreme. To take account of the depletion of gas mass into stars, all the overlap mass in large disruptive collisions was assumed to form into stars and was removed from the cloud system. The overlap mass in glancing collisions could also have been removed, but this contribution was negligible. The third run, with $\epsilon = 20\%$, represents an intermediate situation. In this run the mass of the overlap regions of two clouds involved in a large disruptive collision was reduced by 20%. Since star formation will disrupt the overlap regions, the remainder or 80% of the overlap mass was divided into fragments of $10^4 M_{\odot}$ each. Each fragment was given a new position and velocity away from the center of the cloud created from the overlap regions in much the same way massive clouds are fragmented. Again, for a glancing collision only the overlap mass was kept track of, and the mass was not reduced nor were the overlap regions fragmented. I have also not included the process whereby a fraction of the mass in the stars formed is returned to the interstellar medium via stellar winds and supernova events.

Figure 16 shows the rate at which mass is involved in large collisional disruptions and glancing collisions, \dot{M}_{ovlp} , as a function of time. The plot of \dot{M}_{ovlp} for just large disruptive collisions is essentially the same. From Figure 16 it can be seen that as the star formation efficiency increases the amount of mass involved in disruptive collisions decreases, owing to the conversion of gas mass into stars. The star formation rate, \dot{M}_{*} , for each run is \dot{M}_{ovlp} times ϵ . Thus the curve representing the $\epsilon = 100\%$ case is also the star formation rate. Integrating \dot{M}_{*} over the time interval of the burst of star formation, which was taken to be between the time of closest

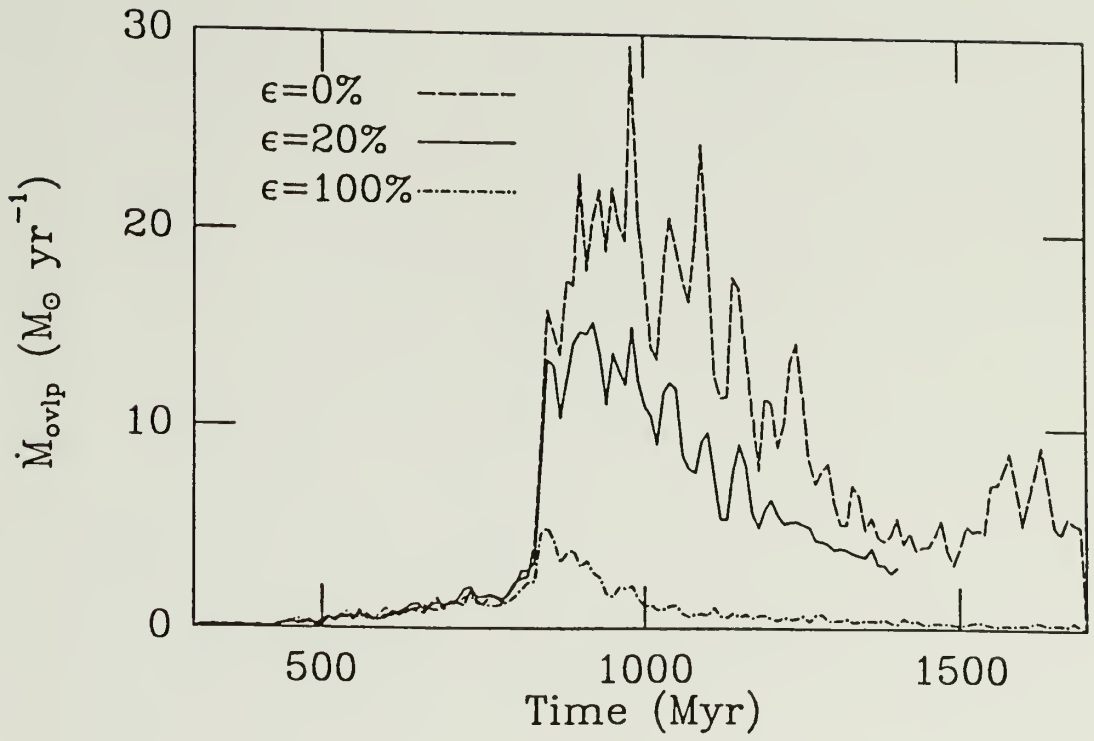


Figure 16 The rate at which mass is involved in large disruptive and glancing collisions as a function of time in case 2. The three curves indicate the results for three different efficiencies at which stars form from the mass involved.

approach and 1400 Myr, the amount of gas turned into stars is obtained. It is $7.5 \times 10^8 M_{\odot}$ and $7.1 \times 10^8 M_{\odot}$ for $\epsilon = 100\%$ and 20% respectively, or roughly one half of the gas mass.

3.2.2 Luminosity to Gas Mass Ratio

With \dot{M}_{*} obtained, the luminosity of the galaxy as a function of time can be calculated by convolving \dot{M}_{*} with an initial stellar mass function (IMF) and the evolutionary tracks for stars (see Searle, Sargent and Bagnuolo [1973] and references therein). It is,

$$L(t) = \int_{m_{\ell}}^{m_u} \int_{t-\tau(m)}^t C(t') \zeta_{*}(m) L_{*}(m, t-t') dm dt'$$

where $L_{*}(m, t-t')$ is the luminosity of a star of mass m at time $(t-t')$ after it forms, $C(t')$ is a normalization constant, m_{ℓ} and m_u are the lower and upper mass limits to stars that are formed, $\zeta_{*}(m)$ is the number of stars formed between mass m and $m + dm$, and $\tau(m)$ is the lifetime of a star of mass m . If $\zeta_{*}(m) = m^{-\alpha}$,

$$C(t') = \dot{M}_{*}(t') \frac{2-\alpha}{m_u^{2-\alpha} - m_{\ell}^{2-\alpha}} .$$

To obtain values for $L_{*}(m, t-t')$ theoretical evolutionary tracks for stars of various masses were obtained from Iben (1965, 1966a, b, c, 1967), Meyer-Hofmeister (1972), Wagner (1974), Lamb, Iben and Howard (1976), Alcock and Pacynski (1978), Brunish and Truran (1982) and Vandenberg (1985). Pre-main sequence tracks were also included and were obtained from Ezer and Cameron (1965, 1967).

Figure 17 shows the luminosity of the galaxy as a function of time due to star formation from disruptive cloud-cloud collisions. The three curves on each plot are for different values of the

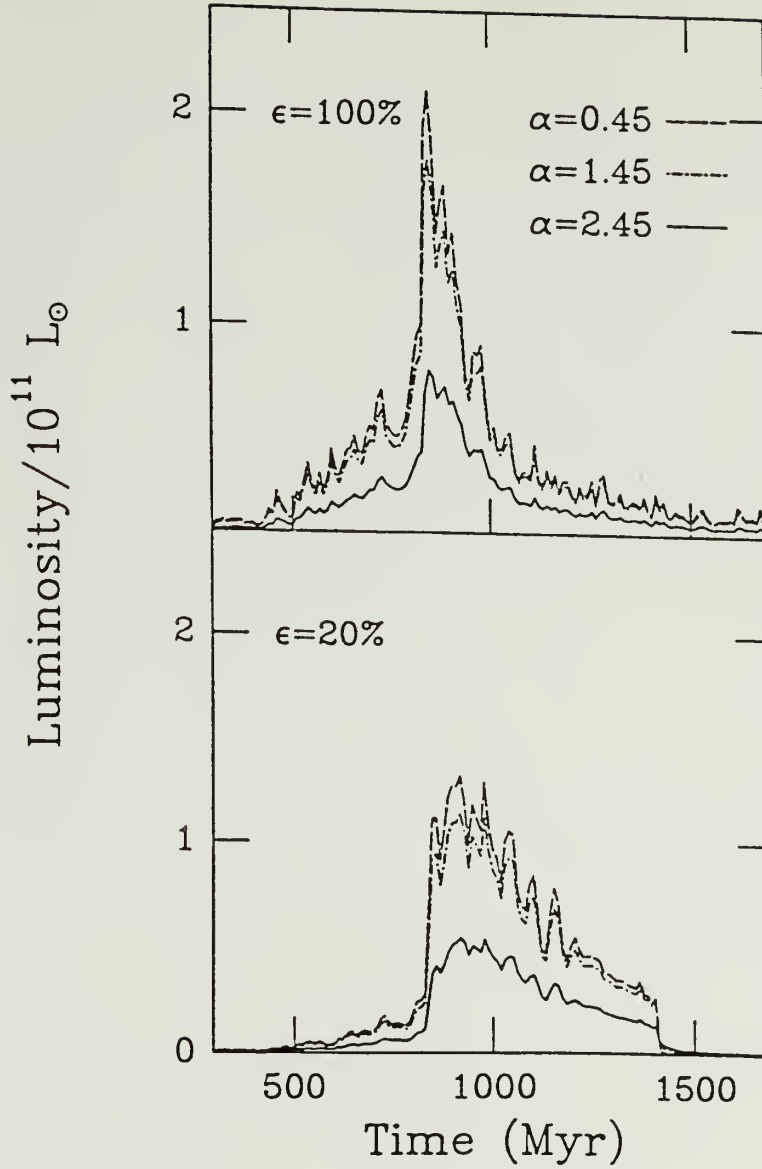


Figure 17 The time dependences of the stellar luminosity produced by the galaxy-galaxy interaction in case 2 for three values of the power law index of the initial stellar mass function. The upper panel shows the result for a 100% efficiency of star formation from the mass involved in disruptive collisions. The lower panel shows the same except for an efficiency of 20%.

parameter α in the IMF. The parameters m_ℓ and m_u are fixed at $0.2 M_\odot$ and $40 M_\odot$ respectively. The Salpeter IMF has $\alpha = 2.45$. Expecting the IMF of stars formed in high velocity cloud-cloud collisions may be weighted toward high mass stars due to the increased Jeans mass in shocked regions, $L(t)$ for $\alpha = 1.45$ and $\alpha = 0.45$ was also determined.

In the case with $\epsilon = 20\%$, $L(t)$ reaches a peak value of $\sim 5 \times 10^{10} L_\odot$ for $\alpha = 2.45$. The luminosity to gas mass ratio is then $5 \times 10^{10} L_\odot / 1.5 \times 10^9 M_\odot$ or $33 L_\odot / M_\odot$. If α is decreased to 1.45 the peak value $L(t)$ reaches is $\sim 1 \times 10^{11} L_\odot$, leading to a luminosity to gas mass ratio of $66 L_\odot / M_\odot$. In the case were $\epsilon = 100\%$ the ratios of luminosity to gas mass are $53 L_\odot / M_\odot$ and $113 L_\odot / M_\odot$ for $\alpha = 2.45$ and $\alpha = 1.45$, respectively. The average value of the infrared luminosity to gas mass ratio for the sample of interacting galaxies of Young et al. (1986b) is $78 L_\odot / M_\odot$. While this small set of experiments precludes definite conclusions about the specific values of ϵ and α , within the context of the model it is noteworthy that $\epsilon \gtrsim 20\%$ and an IMF with a value of $\alpha \leq 2.45$ are required to produce the above mentioned average infrared luminosity to gas mass ratio. Among the uncertainties that could affect the above comparisons between the model results and observational data include the possible contribution to the infrared luminosity from dust heating by a non-thermal continuum source, and the possibility that a fraction of the stellar luminosity may not be obscured by dust and reradiated in the infrared. Also, in the above calculations star formation in massive clouds is not included.

These simulations can also be compared with other observational results. Solomon and Sage (1988) divide their sample of galaxies

into types depending on the distance of separation of the galaxies and the degree of morphological disturbance present in the galaxies. Case 1 shows only a slight morphological disturbance. This places the simulation into Solomon and Sages's (1988) classification scheme as a type 2 interaction where the galaxies show a slight disturbance and no tidal tails. Type 2 interactions show no significant difference from noninteracting galaxies in terms of their infrared luminosity to gas mass ratio. As mentioned earlier, only a slight increase in the star formation rate in case 1 is expected, so this result is consistent with observations. Case 2 fits into the classification of type 3 which consists of the interactions which show large morphological disturbances (i.e. tidal tails and bridges) but are not believed to be merging. For these cases Solomon and Sage (1988) find an average infrared to gas mass ratio of $68 L_{\odot}/M_{\odot}$. The model prediction for this ratio, as described earlier, is consistent with this observational datum. The last case considered is a merger. It falls into the classification of type 4, which comprises galaxies that are believed to be merging. An average infrared luminosity to gas mass ratio of $17 L_{\odot}/M_{\odot}$ is measured, which is considerably lower than that for type 3 interactions. It is notable that case 3 shows a total collisional rate and a rate of large collisional disruptions which, while elevated, are lower than those found in case 2. As pointed out earlier the important parameter is the amount of mass overlap in glancing and large disruptive collisions. With this in mind case 3 was rerun with $\epsilon = 20\%$. A peak \dot{M}_{ovlp} of $10 M_{\odot} \text{ yr}^{-1}$ was obtained. However, this was a very sharp peak near the time of initial close approach, and an average value of $\dot{M}_{\text{ovlp}} = 3-4 M_{\odot} \text{ yr}^{-1}$

was more representative. This gives a luminosity to gas mass ratio of $7.1-9.5 L_{\odot}/M_{\odot}$ if $\alpha = 2.45$ and $14.2-19.0 L_{\odot}/M_{\odot}$ if $\alpha = 1.45$. I should note that among the galaxies classified as types 3 or 4 there is a large degree of scatter in their observed infrared to gas mass ratios (Solomon and Sage 1988). This is especially true of type 4 interactions (mergers) which contain galaxies with some of the highest observed infrared luminosity to gas mass ratios. The present set of models cannot easily account for those merging galaxies which display infrared luminosity to gas mass ratios that are at the extremes. I note, however, that a large amount of parameter space remains to be investigated, such as variations with the parameter γ and the possible presence of gas in the second merging galaxy.

3.2.3 Comparisons with Other Theories

From a theoretical point of view, one may question whether gravitational instability can occur in the overlap regions of two clouds colliding at high velocities (Gilden 1984). However, the situation being described here is probably not too different from the conditions expected to be present in a collapsing protogalaxy. In a protogalaxy the gas clouds are on highly eccentric orbits, and will collide with a speed characteristic of the free-fall velocity. In order to produce the observed present day metallicities and account for the presence of a halo component (Population II), a high rate of star formation in the past is also inferred (Gott 1977). It is suggested that the interaction of two galaxies forces the affected

galaxy into a state similar to that which it had in its early stages of formation.

The models described here show no evidence for limit cycle behavior as suggested by Scalo and Struck-Marcell (1986) and Vásquez and Scalo (1988). They model the cloud system within a galaxy through the application of a set of fluid equations which become unstable when the time scale for the breakup of a massive cloud is comparable to or in excess of the collision time scale, leading to limit cycle behavior. They argue that this limit cycle behavior can lead to repeated bursts of star formation in the disturbed galaxy. In the three simulations described here and in several others in which the time scale for the breakup of a massive cloud is increased to as long as 300 Myr and the evolution of the cloud system was followed to 2.5 billion years after closest approach, this behavior of repeated bursts of star formation is not seen. A situation in which many massive clouds are built up, a burst of star formation follows, the massive clouds are disrupted, and small mass clouds are created which then recombine to form a second generation of massive clouds followed by a second burst of star formation, is not found. Cloud-cloud collisions in a galaxy are stochastic in nature, and the clouds do not behave (i.e. collide, form stars and breakup) in phase with one another. Indeed it can be seen from figures 2-4, 6-8, and 12-14 that during the interaction the relative velocities of collisions range from 0 to high values, and that there are coalescing collisions and formation of massive clouds at the same time as there are disruptive collisions. Thus, the representation of a cloud system by a fluid model in which the mean cloud mass dictates the

rate of star formation for the whole cloud system and in which the mean cloud-cloud velocity dispersion determines whether collisions are coalescing or disruptive (Scalo and Struck-Marcell 1986) may not adequately allow for the broad distributions in both the masses of clouds and the relative velocities of collisions.

It has been suggested by Harwit and Fuller (1988) that the high infrared luminosities associated with interacting and merging galaxies could be produced by dissipation of kinetic energy in the colliding, gaseous disks. The models presented here demonstrate that a large number of high energy gas cloud collisions are produced by the close passage or merger of two galaxies. From the information presented here it is possible to estimate the luminosity produced solely by such gas cloud collisions. Assuming that the kinetic energy in the center of mass system of the two overlap regions in a disruptive collision is all radiated away, the energy thus emitted is no greater than $\frac{1}{8} M_{\text{ovlp}} v_{\text{rel}}^2$, where M_{ovlp} is the sum of the masses in the two overlap regions, and v_{rel} is the relative velocity of collision of the clouds. For case 2 the rate at which mass is involved in large disruptive and glancing collisions, i.e. \dot{M}_{ovlp} , was monitored as a function of time and it reaches a peak of $30 M_{\odot} \text{ yr}^{-1}$. With a typical v_{rel}^2 of $(150 \text{ km s}^{-1})^2$ (c.f. Fig. 8) the maximum expected luminosity due to the dissipation of energy in colliding clouds is then roughly $\sim 1.5 \times 10^7 L_{\odot}$ and the luminosity to gas mass ratio is $0.01 L_{\odot}/M_{\odot}$. Since interacting galaxies are typically observed to have infrared luminosities ranging from $3 \times 10^{10} L_{\odot}$ to $4 \times 10^{12} L_{\odot}$ and an average infrared luminosity to gas mass ratio of $78 L_{\odot}/M_{\odot}$ (Young et al. 1986b) it seems unlikely that enough energy is

liberated solely in cloud-cloud collisions to account for the dramatic infrared luminosities associated with interacting and merging galaxies. It should be pointed out that Harwit and Fuller's (1988) model requires two gaseous disks to be in collision. In the models reported here only one galaxy contains gas and a diffuse gas component which is uniformly distributed has not been included.

Noguchi (1988) shows through a set of N-body experiments that bars can be produced by the close passage of two galaxies. He goes on to show that the formation of such a bar will channel gas into the center of the galaxy leading to increased activity in the center of that galaxy. His final suggestion is that interaction-induced bars are the mechanism by which nuclear star formation activity is caused by the interaction of two galaxies. However, none of the models described here formed an obvious, long-lived bar. Yet, clearly a large amount of activity (large rates of cloud-cloud collision) was induced in the region within 2 kpc of the galactic center. Those models described by Noguchi (1988) which do form a strong, long-lived bar are those which have steeply rising rotation curves out to roughly one half the radius of the disk of the galaxy. The models described here have rotation curves which rise only out to one tenth of the disk radius and become flat thereafter. The model of Noguchi (1988) which most closely resembles those described here in terms of its rotation curve forms only a short transient bar which Noguchi notes is not as efficient at transferring gas to the nucleus of the galaxy as occurred in some of his other simulations. Since the majority of disk galaxies have rotation curves which are relatively flat over 75 percent of the optical disk radius (Rubin et al. 1985),

strong, long-lived bars may not be a preferred outcome of a galaxy-galaxy interaction, nor is it found that the formation of interaction-induced bars is a necessary prerequisite for nuclear star formation activity to be induced by the interaction or merger of two galaxies.

CHAPTER 4

VARIATIONS WITH OTHER PARAMETERS

4.1 Results

In this chapter several additional simulations to those considered in chapter 3 are described. Variations in parameters such as the inclination angle of the interaction, i (the angle between the spin axis of the galaxy which contains gas clouds and the angular momentum vector of the orbit of the two galaxies), the parameter γ (the ratio of the kinetic energy of the two galaxies as measured in the center of mass frame to their gravitational binding energy treating them as mass points), the mass of the perturbing galaxy, and the presence of gas clouds in both galaxies in a case where the galaxies merge, are considered.

First the parameters of the three cases that were simulated in chapter 3 are summarized. In these cases $i = 30^\circ$, $\gamma = 1$, the masses of the galaxy containing gas clouds and the perturbing galaxy are the same and equal $10^{11} M_\odot$, and the impact parameter (b) was decreased from 60 kpc to 40 kpc and then to 20 kpc. These cases are labeled 1, 2, and 3. Here 6 additional cases are considered. Each of the first four cases is identical to case 2 except for one of the above mentioned parameters. Case 4 has $i = 120^\circ$ and can be compared with case 2 to evaluate the difference between a prograde and a retrograde encounter. Cases 5 and 6 consider an unbound and a bound orbit.

Case 5 has $\gamma = 2$ and case 6 has $\gamma = \frac{1}{2}$. In case 7 the mass of the perturbing galaxy is set to $\frac{1}{2}$ the mass of the galaxy which contains gas clouds. In case 8 the effects of having gas clouds in both galaxies when the galaxies merge are considered. For this simulation the orbital parameters are the same as those in case 6. A final case, case 9, is also considered which is identical to case 8 except that the total amount of gas is halved. A list of the model parameters in each of the cases 1-9 is given in Table 1. In performing these simulations we hope to understand some of the scatter in the observed $L_{\text{IR}}/M_{\text{H}_2}$ ratios (e.g., Young et al. 1986 a,b; Solomon and Sage 1988).

In case 4 the galaxies reach a distance of closest approach of 13 kpc at a time of 900 Myr after the start of the simulation. The morphological changes induced by the interaction are not as pronounced as in case 2 but more so than in case 1 (Fig. 18). It is unclear whether the structures (at 1100 Myr for instance) would be considered bridges or tails. This consideration places this interaction as intermediate between types 2 and 3 in the classification scheme suggested by Solomon and Sage (1988).

The total rate of cloud-cloud collisions, the rate of cloud coalescence, the rate of large collisional disruption, and the rate of production of fragments due to star formation in massive clouds (in the region of the galaxy exterior to 2 kpc from the galactic center) are shown as a function of time in Fig. 19. The total rate of cloud-cloud collisions comprises the rate of cloud coalescence, the rate of large collisional disruption, and the rate of glancing collisions. It does not begin to increase immediately after closest

Table 1
Parameters for all Models

Case	b(kpc)	γ	i	M_p/M_{gal}	Interaction	$M_{gas} (10^9 M_\odot)$
1	60	1	30°	1	type 2	1.5
2	40	1	30°	1	type 3	1.5
3	20	1	30°	1	merger	1.5
4	40	1	120°	1	type 2-3	1.5
5	40	2	30°	1	type 3	1.5
6	40	$\frac{1}{2}$	30°	1	merger	1.5
7	40	1	30°	$\frac{1}{2}$	type 3	1.5
8	40	$\frac{1}{2}$	30°	1	merger	3
9	40	$\frac{1}{2}$	30°	1	merger	1.5

Notes: see text for the definitions of b, γ and i

M_p = mass of perturbing galaxy

M_{gal} = mass of galaxy containing gas clouds

M_{gas} = total mass of gas

The types of interaction refer to the classes of interacting galaxies defined by Solomon and Sage (1988).

Cases 6, 8, and 9 have the same parameters for the interaction. The difference is that in cases 8 and 9 both galaxies contain an equal amount of gas.

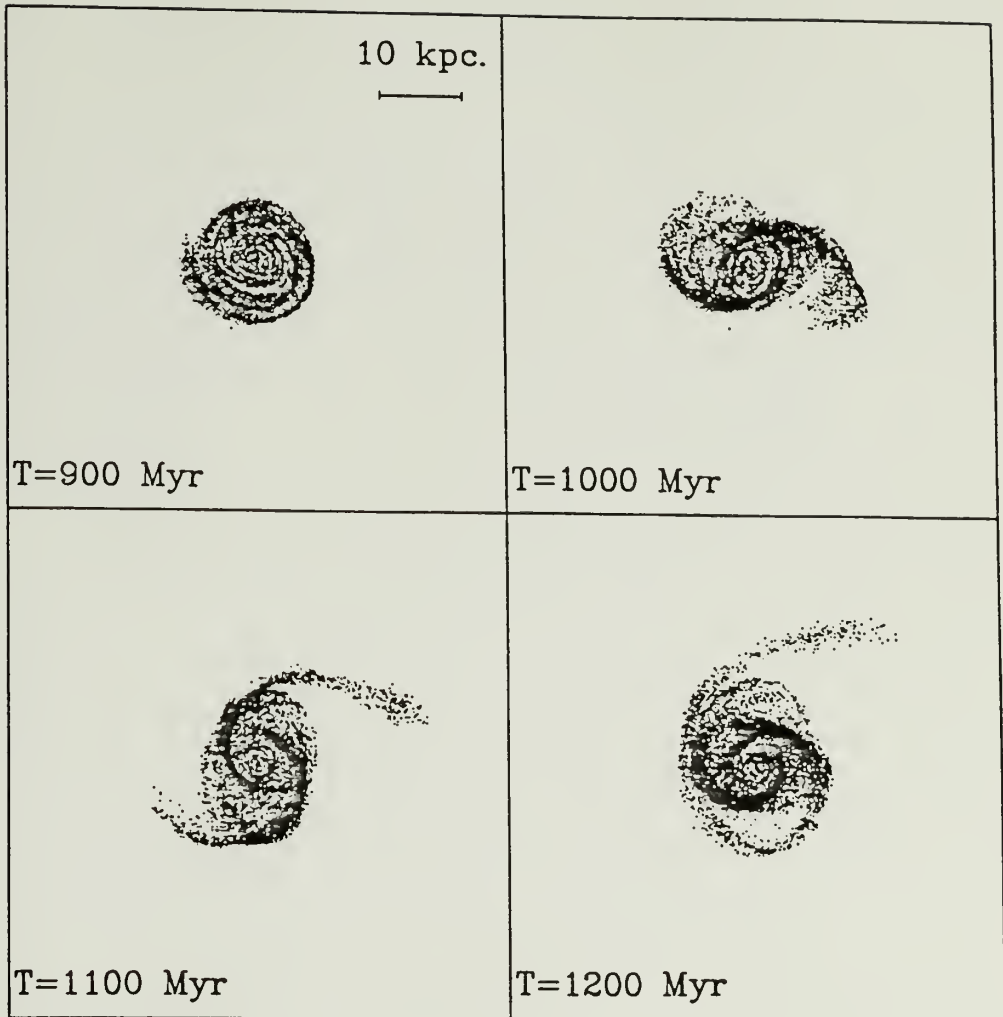


Figure 18 The morphological change of the cloud system for case 4 ($i = 120^\circ$). Closest approach occurs at 900 Myr and the distance of closest approach is 13 kpc. All views are face-on in the rest frame of the galaxy.

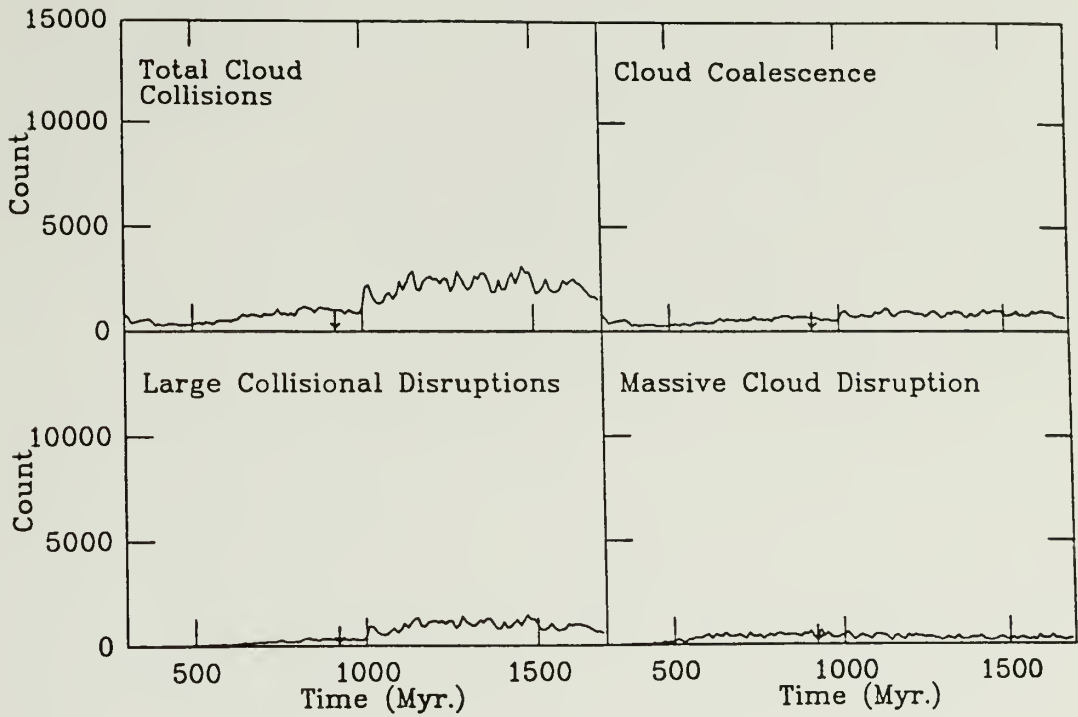


Figure 19 Time dependences for case 4, in the region exterior to 2 kpc of the galactic center, of the total rate of cloud-cloud collision (in units of number per 10 Myr), the rate of coalescence, the rate of large collisional disruptions, and the rate at which fragments are produced due to star formation in massive clouds.

approach as in previous cases, but does rise above the unperturbed value by a factor of ~ 2.5 . The rate of cloud coalescence remains relatively unaffected. On the other hand, the rate of large collisional disruptions is raised by a factor of ~ 4 and comprises 40% of the total rate. As in chapter 3, most of the collisions which are induced to occur by the interaction are large disruptive or glancing collisions and do not lead to the production of a large number of massive clouds ($\geq 10^6 M_{\odot}$). Thus, no increase in the rate at which fragments are produced as a result of star formation in massive clouds is seen. In the region interior to 2 kpc from the galaxy's center no significant increase in any of the collisional rates is noted.

The velocity spectra are similar to those in previous cases. They do not reflect a large perturbation and do not extend much beyond 100 km s^{-1} . The mass spectra are not affected much by the interaction.

The next case considered (case 5) is one with $\gamma = 2$. The morphological changes are shown in Fig. 20. The galaxies reach a distance of closest approach of 19 kpc at a time of 925 Myr. Even though tails and bridges do form, they are not as extended as in case 2. By the end of the calculation a ring in the gas distribution with a surface density roughly 1.5 times the unperturbed value forms between a radius of 4 and 6 kpc from the center of the galaxy.

The collisional rates of interest are shown in Fig. 21 for the region of the galaxy exterior to 2 kpc from the galactic center. At its peak the total rate of collisions in this region is raised above its unperturbed value by a factor of ~ 6 . At the same time the rate

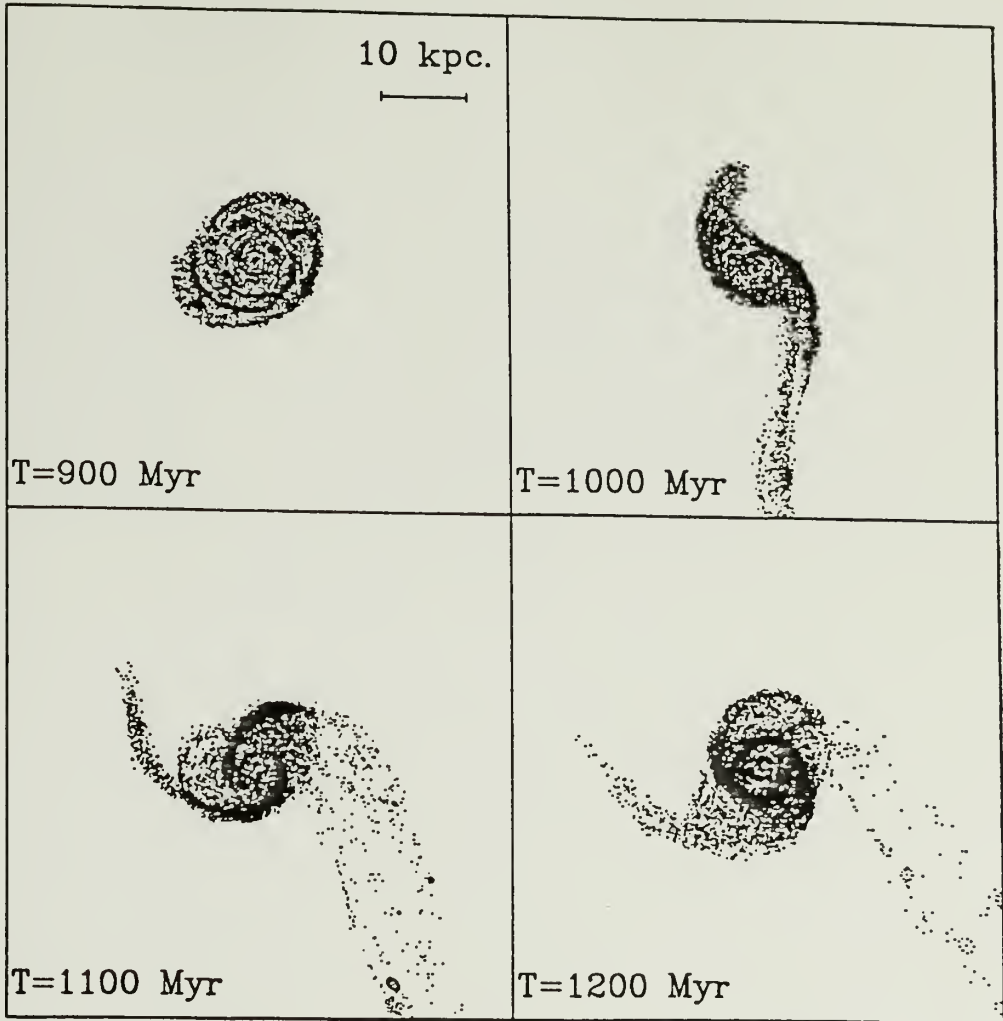


Figure 20 Same as Fig. 18 except for case 5 ($i = 30^\circ$, $b = 40$ kpc, and $\gamma = 2$). Closest approach occurs at a time of 925 Myr and the distance of closest approach is 19 kpc.

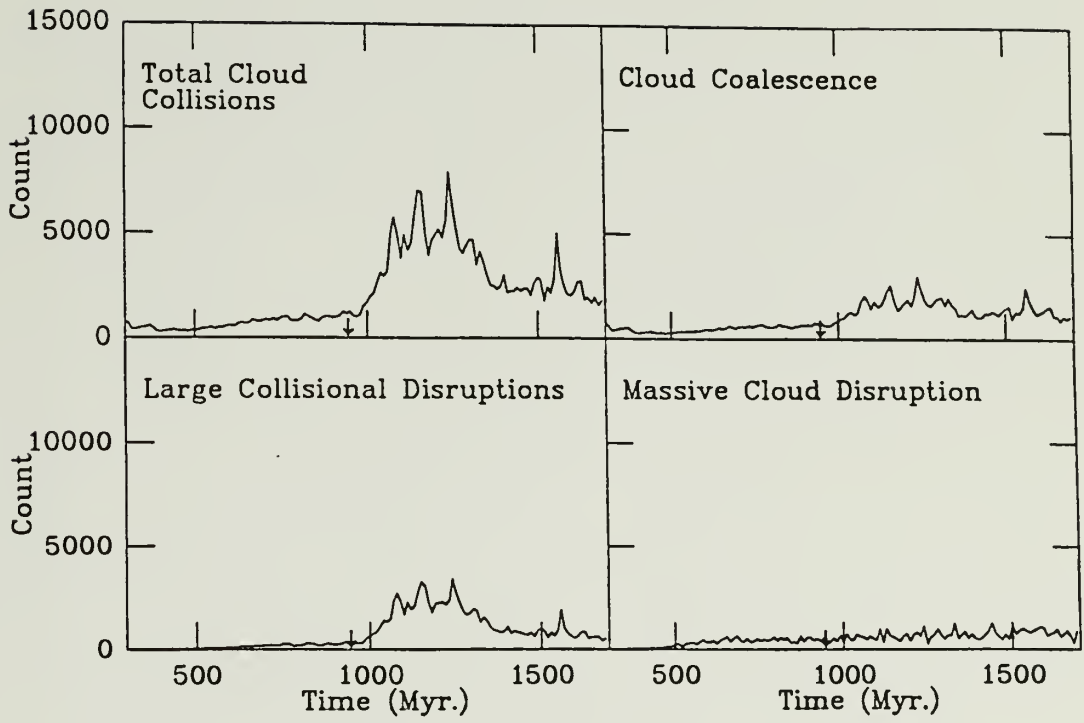


Figure 21 Same as Fig. 19 except for case 5.

of coalescence is raised by a factor of ~ 3 while the rate of large collisional disruptions is raised by a factor of ~ 10 . Again, the rate at which fragments are produced due to star formation in massive clouds is raised by no more than a factor of 1.5. In the region of the galaxy interior to 2 kpc from the center of the galaxy none of the rates (after the time of closest approach) is appreciably different from its unperturbed value.

The distribution of collisional velocities becomes quite broad as a result of the interaction, extending to $\sim 200 \text{ km s}^{-1}$. The mass spectrum of clouds responds as in case 2 by becoming flatter with a few more clouds that are more massive than $10^6 M_{\odot}$ and many more clouds that are less massive than $10^5 M_{\odot}$ being produced.

The next case (case 6) considered was one with $\gamma = \frac{1}{2}$ (a bound orbit). When compared to case 5, reducing the value of γ amounts to reducing the relative velocity of the two galaxies.

In this case the galaxies merge as in case 3. As a result, the morphology of the galaxies is severely disturbed. Tails and bridges appear soon after the initial close approach of the density centers of the two galaxies which occurs at 832 Myr. These changes are shown in Fig. 22 for the face-on view and Fig. 23 for the edge-on view. After their initial close approach the galaxies merge roughly 400 Myr thereafter (i.e. the distance between the density centers of the galaxies is near zero and remains so for the rest of the calculation).

As in the previous case considered where the galaxies merge (case 3), no large increase in the total rate of cloud-cloud collisions in the region exterior to 2 kpc of the galactic center was

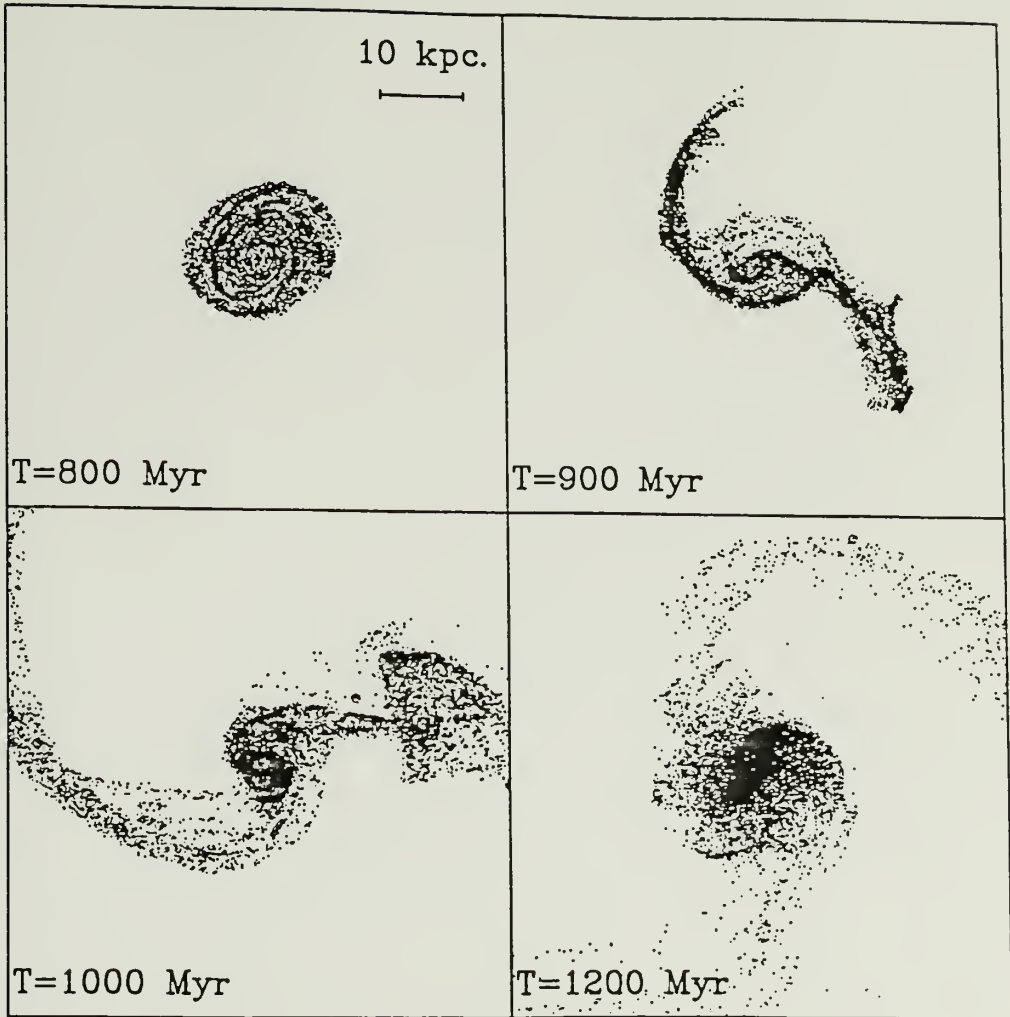


Figure 22 Face-on view of the morphological change of the cloud system in case 6 ($i = 30^\circ$, $b = 40$ kpc, and $\gamma = 1/2$) where the galaxies merge.

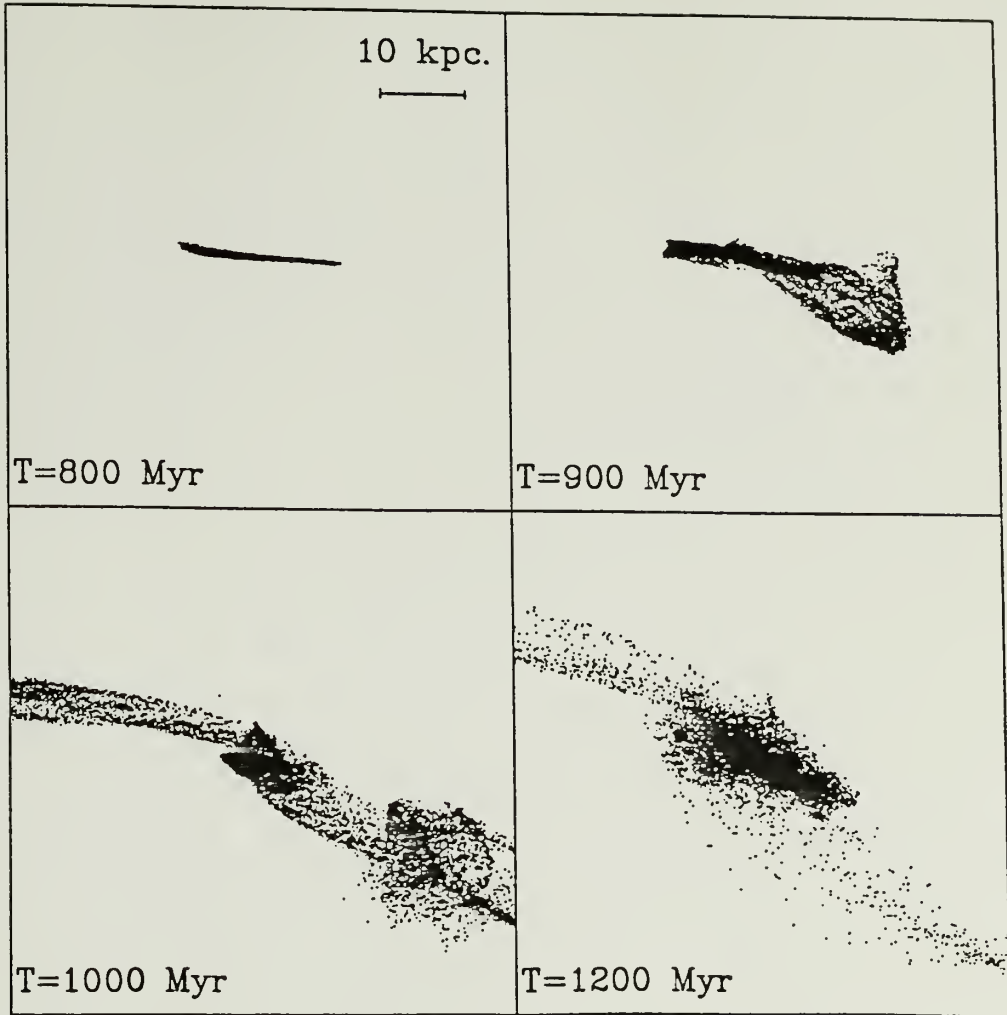


Figure 23 Edge-on view of the cloud system for case 6.

seen but a dramatic increase is seen in the inner galaxy. The relevant collisional rates are shown in Fig. 24 for the region of the galaxy interior to 2 kpc from the galactic center (note the different scales in Fig. 24). In this region the total rate of cloud-cloud collisions is raised above its unperturbed value by a factor of ~ 10 shortly after the initial close approach of the galaxies. As the galaxies merge 400 Myr after the initial close approach, a second increase in the total rate of cloud-cloud collisions is seen. Here, the rate is elevated above its unperturbed value by a factor of ~ 120 .

For the rate of cloud coalescence it is seen that exterior to 2 kpc this rate drops after the initial close approach of the two galaxies. Interior to 2 kpc, it is raised by a factor of ~ 3.5 shortly after the initial close approach and coalescing collisions comprise $\sim 40\%$ of the total number of collisions. At the time when the total rate of cloud-cloud collisions undergoes its second burst the coalescence rate is raised above its unperturbed value by a factor of ~ 10 ; however, coalescing collisions now comprise only 10% of the total number of collisions.

Once again glancing and large disruptive collisions constitute the majority of the cloud-cloud collisions induced by the interaction. After the initial close approach the rate of large collisional disruptions is raised above its unperturbed value by a factor of ~ 30 . At the time when the galaxies merge and the total collisional rate undergoes a second burst, the rate of large disruptive collisions is raised above its unperturbed value by a factor of ~ 200 and glancing and large disruptive collisions comprise

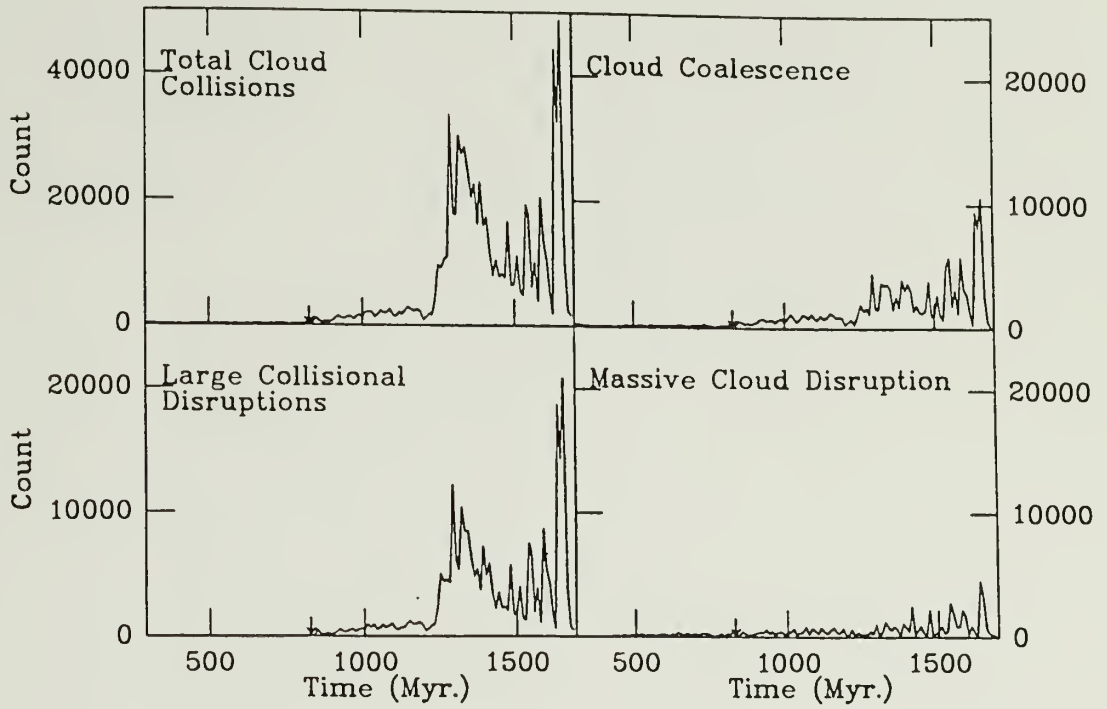


Figure 24 Same as Fig. 19 except plots are for the region interior to 2 kpc for case 6. Note the different scales for each plot.

90% of the total number of cloud-cloud collisions. This is by far the largest increase seen among the cases considered so far.

The rate at which fragments are produced due to star formation in massive clouds also shows two increases. It is raised at the time of initial close approach by a factor of $\lesssim 1.5$ in the region interior to 2 kpc. After the second rise in the other rates, it is raised at times by a factor of ~ 10 above its unperturbed value. However, it is very nonuniform. This is because a small number of very massive clouds (~ 10) form near the center of the merger remnant (see below). When averaged over time, the mass of gas involved in disruption of massive clouds due to star formation does not rise above the unperturbed value by a factor of more than 3.

The velocities at which the clouds collide are once again raised by the interaction and the distribution of collisional velocities becomes very broad as a result of the merger of the two galaxies. Typical collisional velocity distributions are similar to those seen in case 3.

During the initial increase in the rates mentioned above, the mass spectra show no large changes with time. However, after the time the galaxies merge several large clouds with masses $> 10^7 M_{\odot}$ form. All of these clouds are located within 1 kpc of the center of the merger remnant and most of them are within 0.5 kpc. As mentioned in chapter 2, if the masses of two colliding clouds are very different, the condition for coalescence is dominated by the internal binding energy of the larger cloud. Hence, a very massive cloud can accrete a large amount of mass even if the relative velocities of the smaller clouds colliding with it are large. Even when the second

criterion for coalescence as described in chapter 2 is used, very massive clouds are still formed.

To determine how the mass of the perturbing galaxy affects the results, case 7 is run with the mass of the perturbing galaxy reduced to $\frac{1}{2}$ the mass of the galaxy which contains gas clouds. The morphological changes are shown in Fig. 25. In this case the distance of closest approach is 12 kpc and tails and bridges form near the time of closest approach (900 Myr).

The rates of interest are shown in Figs. 26 and 27 for the regions of the galaxy exterior and interior to 2 kpc from the galactic center respectively. The rates are increased in both regions of the galaxy as a result of the interaction, with the rate of large disruptive collisions increasing the most, and the rate at which fragments due to star formation in massive clouds increasing the least. However, the increases are slightly smaller than those seen in case 2.

The distribution of collisional velocities becomes quite broad, extending to velocities of $\sim 200 \text{ km s}^{-1}$. The mass spectrum of clouds once again flattens out with both small clouds and clouds more massive than $10^6 M_{\odot}$ being produced.

In case 8 the effects caused by the presence of gas in both galaxies when they merge are considered. Here the orbital parameters are the same as those used in case 6 above. As the galaxies merge their morphologies are severely disturbed and are shown in Figs. 28 and 29. The disk of each galaxy is disrupted, leading to the formation of an elliptical-like object after the time of merging.

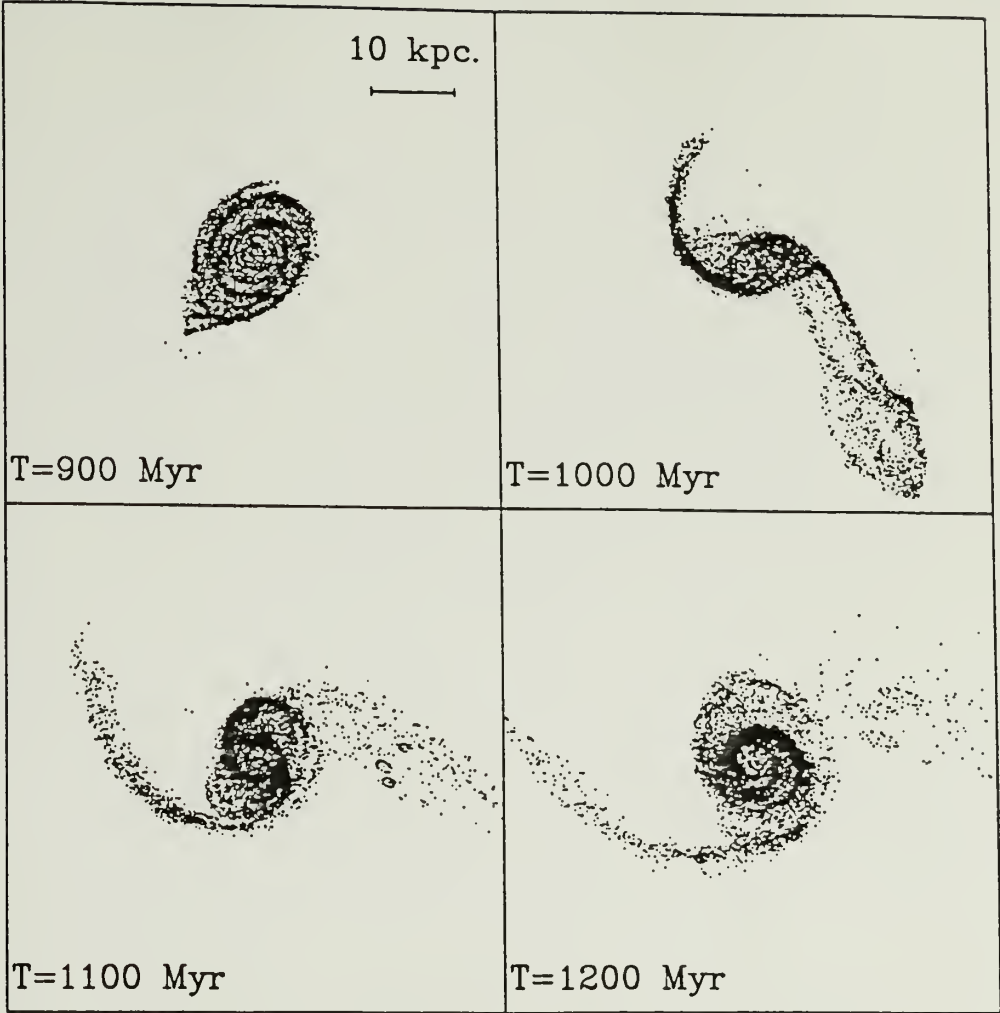


Figure 25 Same as Fig. 18 except for case 7 (perturber mass is $1/2$ galaxy mass). Closest approach occurs at a time of 900 Myr and the galaxies come to within 12 kpc.

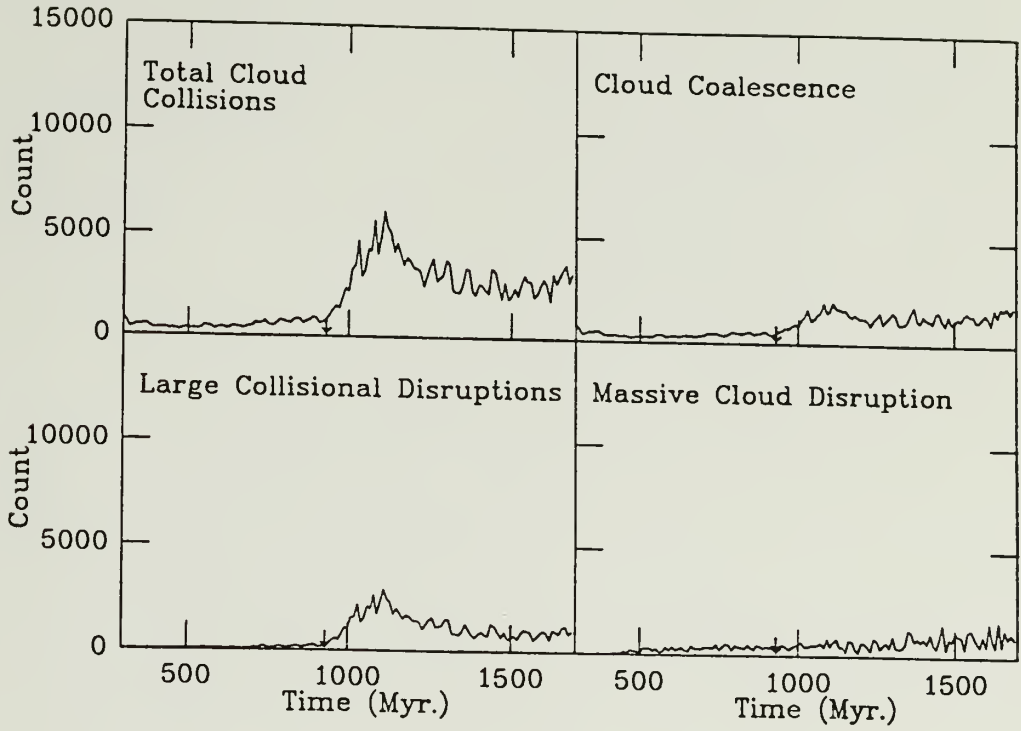


Figure 26 Same as Fig. 19 except for case 7.

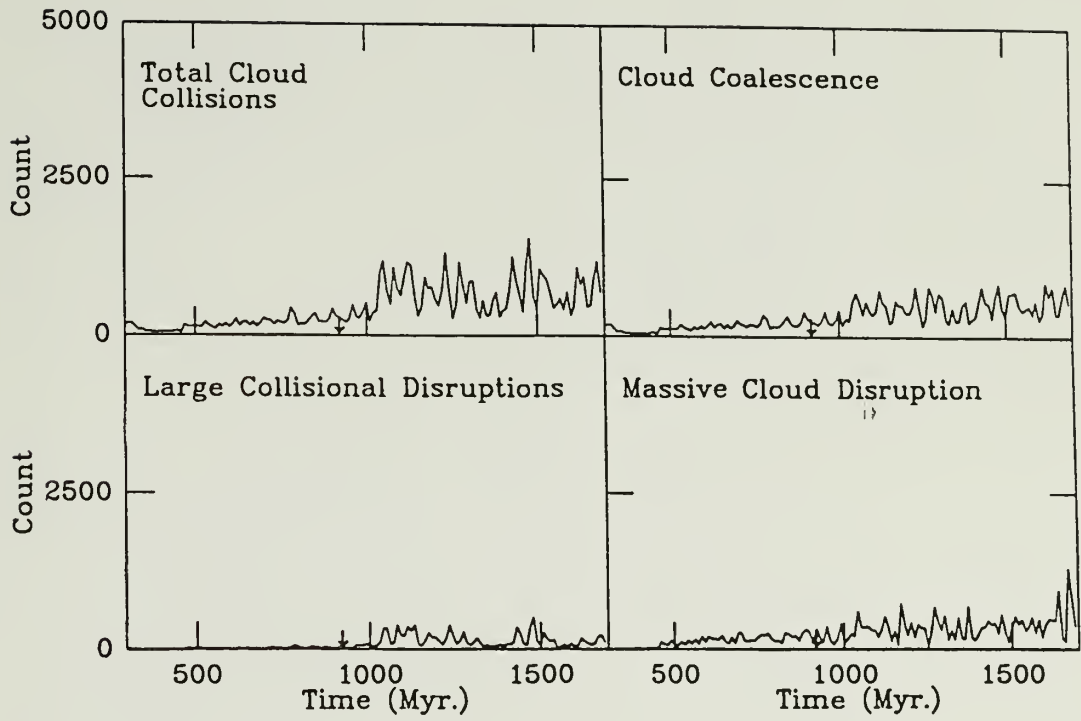


Figure 27 Same as Fig. 24 (region less than 2 kpc) except for case 7.

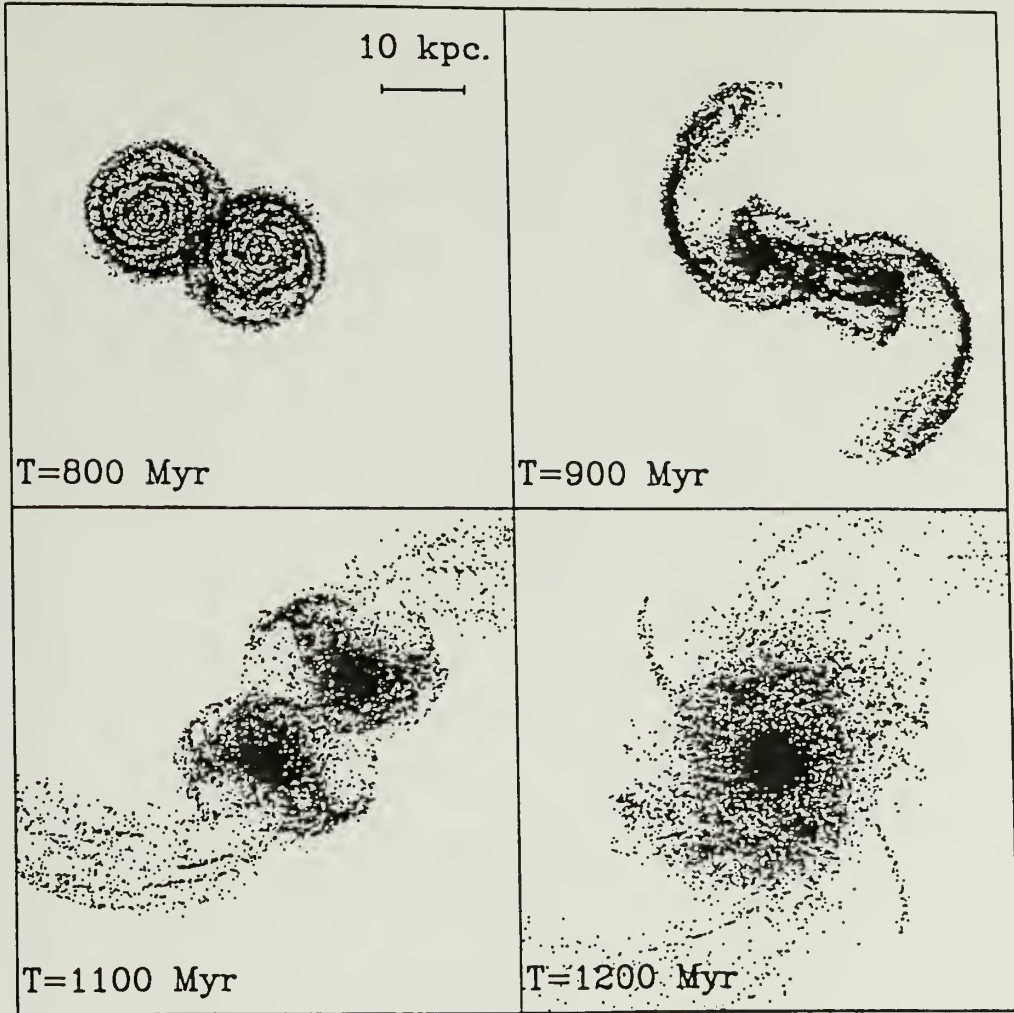


Figure 28 Same as Fig. 18 except for case 8. All views are in the rest frame of one of the galaxies.

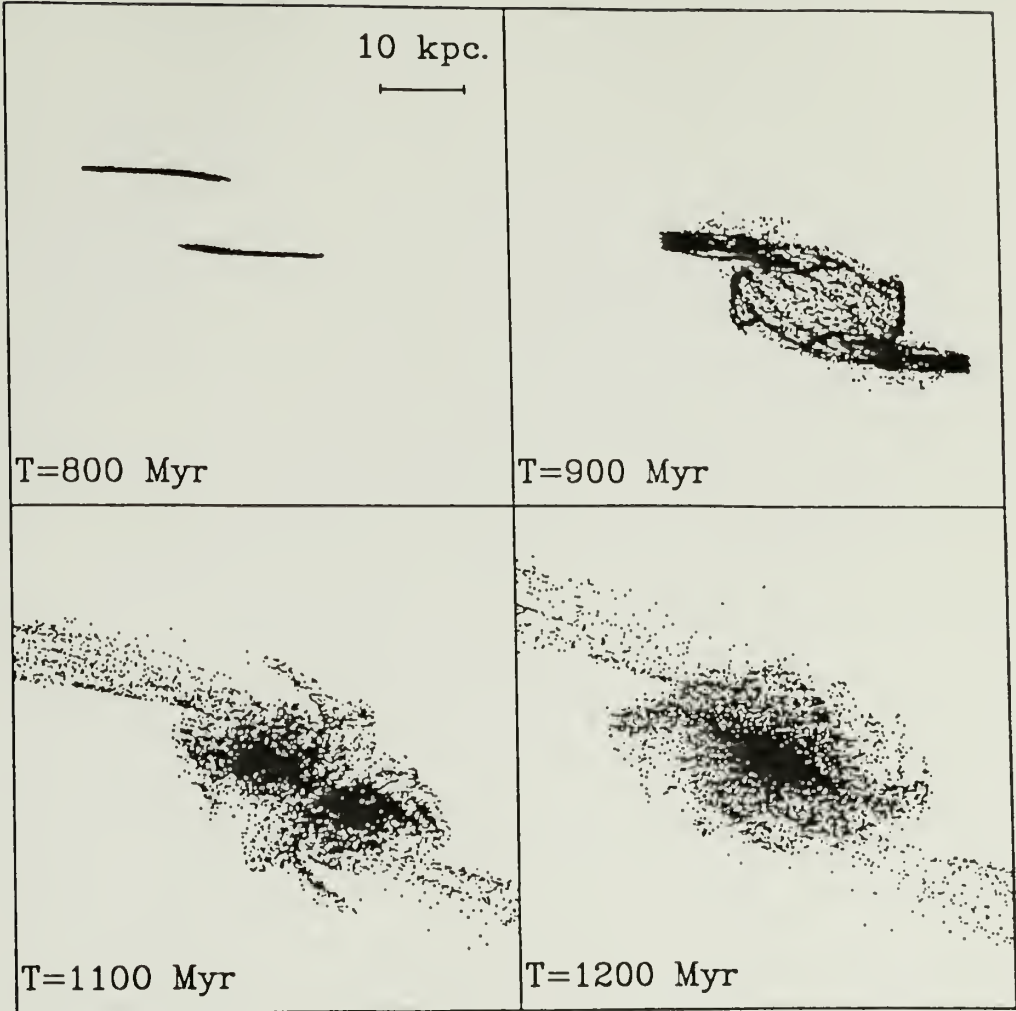


Figure 29 Same as Fig. 23 except for case 8.

The total rate of cloud-cloud collisions in the region of the galaxy exterior to 2 kpc is similar to that seen in case 6. Here, in order for a collision to be considered exterior to 2 kpc it must have occurred at a distance in excess of 2 kpc from the center of each galaxy, otherwise it is counted as a collision in the region interior to 2 kpc.

Within a distance of 2 kpc from the center of either galaxy the rates are severely affected and are shown in Fig. 30. The total rate of cloud-cloud collisions is raised by a factor of ~ 10 above its unperturbed value soon after the initial close approach. When the galaxies merge, it undergoes a second increase which, at its peak, is ~ 150 times higher than the unperturbed value. The rate of coalescence also rises steadily after the initial close approach and is raised by a factor of ~ 20 (and comprising 10% of the total number of collisions) at the time of merging. The rate of large collisional disruptions increases the most rapidly; it is raised by a factor of ~ 500 at the time of merging. The rate at which fragments are produced due to disruption of massive clouds by star formation remains nearly the same at the initial close approach but is raised by a factor of ~ 7 after the time of merging. This increase is less than that seen in case 6, indicating that large disruptive and glancing collisions are even more important here.

The distributions of collisional velocities are shown in Fig. 31 at four different times for the region interior to 2 kpc. The velocities with which the clouds collide are very high in this case, extending to 500 km s^{-1} . As the calculation proceeds after the

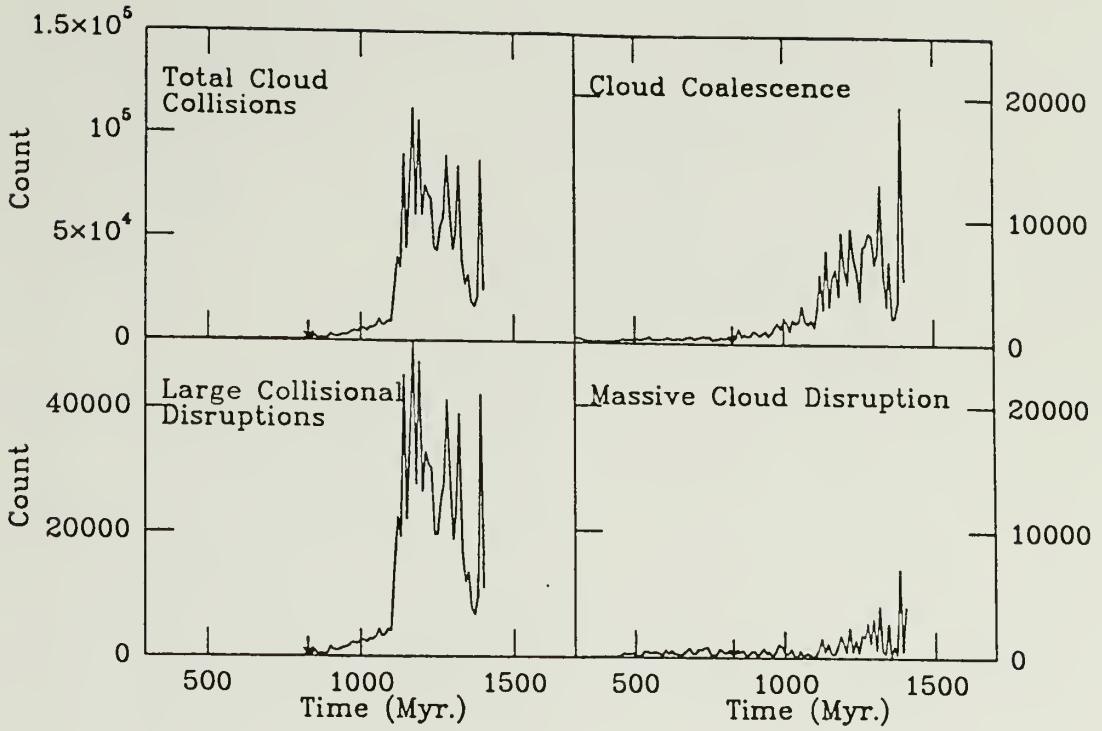


Figure 30 Same as Fig 24 (region less than 2 kpc) except for case 8. Note the different scales on each plot.

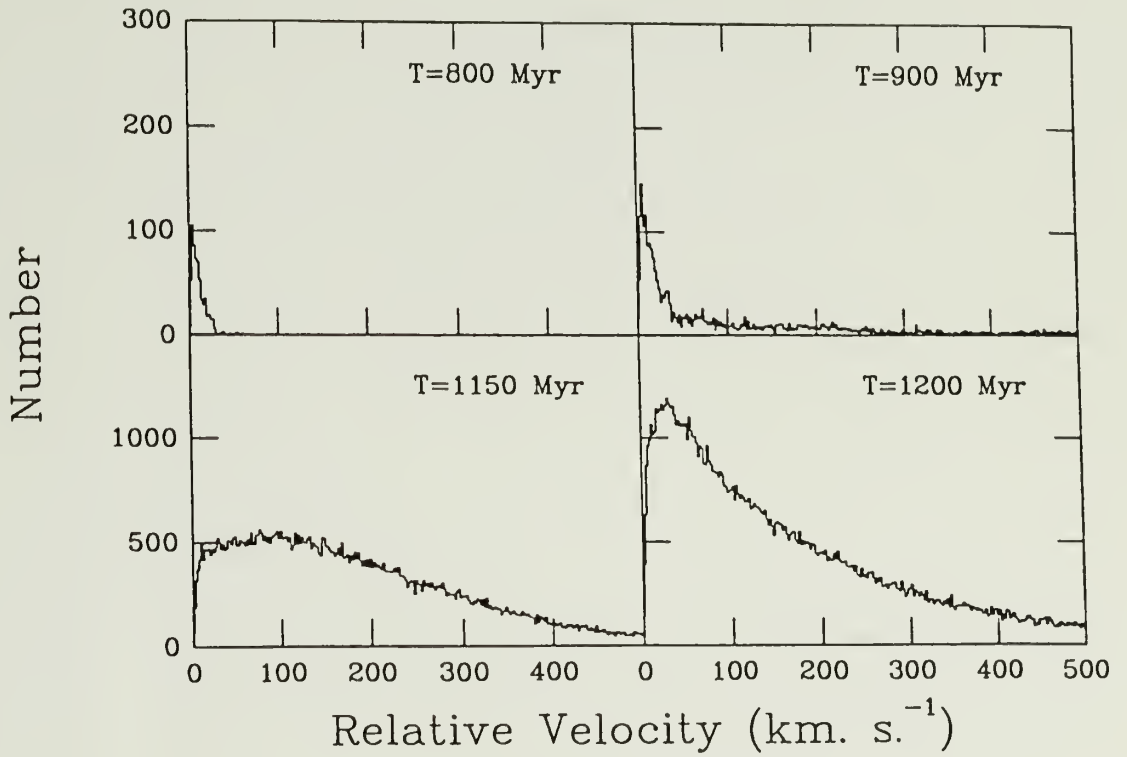


Figure 31 Distributions of the relative velocities of the cloud-cloud collisions at four different times for case 8. All views are for those collisions occurring within 2 kpc of the center of either galaxy.

galaxies have merged, the distribution of collisional velocities narrows and coalescing collisions become relatively more frequent.

The mass spectrum of clouds is characterized by the production of many small clouds after the time the galaxies merge. Unlike case 6, no very massive clouds ($> 10^7 M_{\odot}$) were formed at any time. This indicates that disruptive collisions were frequent enough to prevent the build up of such massive clouds. However, since the velocity distribution narrows with time, an increased rate of coalescence at later times could lead to the formation of massive clouds. This can only occur at $\gtrsim 600$ Myr after the initial close approach or $\gtrsim 300$ Myr after the galaxies merge, well beyond the time when obvious tails and bridges are present.

4.2 Discussion

The effects each of the model parameters has on the galaxy-galaxy interaction are summarized in this section. The implications they have for the star formation process in interacting and merging galaxies are also discussed, and comparisons with available observations are made.

First, increasing the inclination of the interaction reduces the perturbation placed upon the galaxy which contains gas clouds. This is reflected in the morphological changes which are induced, in the total rate of cloud-cloud collisions after closest approach, and in the relative fraction of disruptive collisions. In case 2 ($i = 30^{\circ}$) the rate of large collisional disruptions is raised by a factor of ~ 18 in the region of the galaxy exterior to 2 kpc and by a factor of

~ 30 in the region interior to 2 kpc. In case 4 ($i = 120^\circ$) the rate of large collisional disruptions was raised above the unperturbed value (at its peak) by a factor of only 4 in the region exterior to 2 kpc and was not effected in the inner region. A third case with $i = 60^\circ$ was also considered. Here the restricted three body approximation was used to find the acceleration of each cloud particle. The results, in terms of morphology and cloud-cloud collisional rates, are intermediate between those found in cases 2 and 4.

These results are consistent with those of Noguchi and Ishibashi (1986) who considered prograde and retrograde orbits and found that retrograde orbits induce less of a perturbation and a smaller number of cloud-cloud collisions than prograde orbits. Solomon and Sage (1988) classify interacting galaxies according to the degree of morphological disturbance present in a galaxy and its proximity to another galaxy. In this classification scheme case 2 was indentified as a type 3 interaction (bridges and tails present but not merging) and a peak $L_{\text{IR}}/M_{\text{H}_2}$ of $\sim 66 L_\odot/M_\odot$ was obtained (assuming the power law index of the initial mass function is $\alpha = 1.45$ and the efficiency for star formation is $\epsilon = 20\%$). The average value measured by Solomon and Sage (1988) for type 3 interactions is $68 L_\odot/M_\odot$ with the lowest value among this subset of interacting galaxies being $25 L_\odot/M_\odot$. In case 4 there are clear morphological disturbances, and although tail-like structures are seen, bridges or tails as dramatic as those in case 2 never form. Therefore, this case is classified as intermediate between types 2 and 3. Type 2 interactions are observed

to have an average $L_{\text{IR}}/M_{\text{H}_2}$ ratio of $7.8 L_{\odot}/M_{\odot}$, with the maximum value among this subset of interacting galaxies being $28 L_{\odot}/M_{\odot}$ (Solomon and Sage 1988). The $L_{\text{IR}}/M_{\text{H}_2}$ ratio can be estimated for case 4 as was done for case 2. Assuming $\alpha = 1.45$ and $\epsilon = 20\%$, an average $L_{\text{IR}}/M_{\text{H}_2}$ ratio of $\sim 26\text{-}30 L_{\odot}/M_{\odot}$ is obtained for case 4. Hence, this case also represents a transition between types 2 and 3 in terms of its star forming properties.

Three orbits varying the parameter γ have been considered in chapter 3 and here. In case 5 ($\gamma = 2$) the morphology is severely disturbed, although the tails and bridges formed are not as extended as in case 2. Here, the rate of large collisional disruption rises by a factor of ~ 10 in the region exterior to 2 kpc, but none of the rates of interest is noticeably affected in the region interior to 2 kpc. I also note that in this case a ring-like density enhancement is formed between 4 and 6 kpc from the center of the galaxy, hence most of the cloud-cloud collisions occur there and I would predict that the most intense star formation induced by the interaction will be located there. This case and also case 4 indicate that all interacting galaxies which show morphological peculiarities associated with an interaction need not have star formation induced only in or near their nuclei. Although, based on the results presented here and in chapter 3, it is expected that the majority of interactions which produce tails and bridges will have star formation induced near their centers.

Bushouse (1986), who considers only violently interacting galaxies with clear morphological disturbances, finds that most of them have star formation rates which are elevated only in or near the

centers of the perturbed galaxies. He also finds that a fraction (~ 30% of his sample) show no detectable, nuclear star formation but that a number of these galaxies have H α fluxes which peak some distance away from the center of the galaxy or fluctuate around a constant level throughout the disk of the galaxy. Kennicutt et al. (1987) observe that many of the interacting galaxies in their sample can also have significant amounts of star formation induced in their disks as well as in their central regions. The results for cases 4 and 5 are consistent with these observations.

When the value of γ is reduced to $\frac{1}{2}$ the galaxies merge. The morphology is severely disturbed and, as in the previous merging case considered (case 3), virtually all of the activity induced by the merger is confined to the region of the galaxy interior to 2 kpc. As noted earlier, the cloud-cloud collisional rates undergo two increases, one at the time of initial close approach and one at the time of merging. The second increase is accompanied by the formation of several (~ 10) very massive clouds. If the formation of such clouds leads to a burst of star formation, then it would appear only after a period of 400 Myr since the initial close approach. If, however, a burst of star formation is induced at or near the time of initial close approach and is not delayed, then the star formation which is induced may be related to the large number of large disruptive and glancing collisions.

To test whether the formation of very massive clouds which is noted in case 6 can lead to a burst of star formation this case has been rerun and the amount of gas mass involved in the disruptions of massive clouds due to star formation, \dot{M}_{drpt} , has been monitored.

Again the parameter ϵ is specified as the efficiency of star formation or the fraction of the gas which is converted into stars. Therefore, each time a massive cloud is disrupted, the amount of mass returned to the interstellar medium in fragments is $(1-\epsilon)$ times the mass of the original cloud. The parameter ϵ is set equal to 10% so that the unperturbed galaxy has a luminosity to gas mass ratio roughly equal to the observed $L_{\text{IR}}/M_{\text{H}_2}$ of noninteracting galaxies. In this case, the plot of \dot{M}_{drpt} as a function of time does not show the several-fold increase in the rate of production of fragments due to star formation in massive clouds seen in case 6 (c.f. Fig. 24). Instead it does not rise much above its unperturbed value due to the fact that the gas mass is continually being depleted. Thus, no burst of star formation is found in this test.

To estimate the increase in the star formation rate and the consequent increase in luminosity of the galaxy due to large disruptive and glancing collisions, case 6 was rerun a third time with $\epsilon = 20\%$. The star formation rate in this case is $\epsilon \cdot \dot{M}_{\text{ovlp}}$, with \dot{M}_{ovlp} being the rate at which mass is involved in disruptive and glancing collisions. The luminosity of the galaxy is also found as described in chapter 3. In Fig. 32 the luminosity to gas mass ratio, taking into account the continual depletion of gas due to star formation, is shown as a function of time for $\alpha = 2.45, 1.45,$ and 0.45 respectively. A characteristic value of $\sim 30 L_{\odot}/M_{\odot}$ is reached when $\alpha = 1.45$ or 0.45 . The average value for type 4 interactions (mergers) found by Solomon and Sage (1988) is 17.

Next, the effect of the mass of the perturbing galaxy is considered. The perturbation is reduced by decreasing the mass of

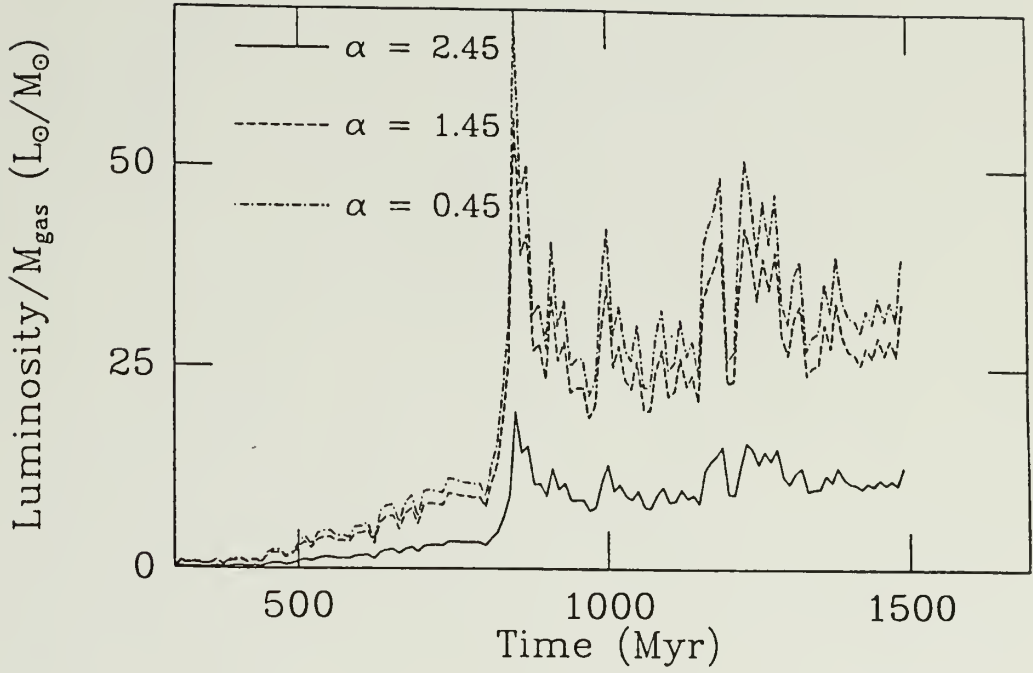


Figure 32 The luminosity to gas mass ratio as function of time for case 6 with $\epsilon = 20\%$ taking into account the depletion of gas due to star formation for $\alpha = 2.45, 1.45$ and 0.45 .

the perturber. This is reflected in both the morphological changes induced by the interaction and in the rise in the total cloud-cloud collisional rate after closest approach. In this case a peak luminosity to gas mass ratio of $\sim 20 L_{\odot}/M_{\odot}$ is produced due to star formation in large disruptive and glancing collisions.

In case 8 the presence of gas in both galaxies when they merge is considered. As in case 6 the rates are not appreciably affected in the region of the galaxies exterior to 2 kpc and all the activity is located within 2 kpc of the center of each galaxy.

Harwit and Fuller (1988) suggest that the high infrared luminosities associated with merging galaxies can be explained by the dissipation of energy in the collision of the gaseous components of the galaxies. In case 8 a peak \dot{M}_{ovlp} of $150 M_{\odot} \text{ yr}^{-1}$ is reached. The rate of dissipation in large disruptive and glancing collisions is then $\frac{1}{8} \dot{M}_{\text{ovlp}} v_{\text{rel}}^2$. Taking a typical collisional velocity of 300 km s^{-1} , a luminosity of $3 \times 10^8 L_{\odot}$ is produced with a luminosity to gas mass ratio of $0.1 L_{\odot}/M_{\odot}$. Even for a maximum v_{rel} of 500 km s^{-1} (see Fig. 31) a $L_{\text{IR}}/M_{\text{H}_2}$ of only $0.3 L_{\odot}/M_{\odot}$ is reached. Interacting and merging galaxies are observed to have an average far infrared luminosity to gas mass ratio of $\sim 78 L_{\odot}/M_{\odot}$ (Young et al. 1988b). Hence the far infrared luminosities associated with interacting and merging galaxies cannot be explained solely by the dissipation of energy due to the collision of two gaseous galactic disks and stars must be formed.

Case 8 was rerun with $\epsilon = 20\%$, primarily to see if the highest observed values of $L_{\text{IR}}/M_{\text{H}_2}$ could be reproduced. Here the total rate of cloud-cloud collisions, and the rate of large collisional

disruptions undergo increases at the time of initial close approach similar to those in the original case ($\epsilon = 0\%$). These rates also undergo a second increase when the galaxies merge, but the increases are not as large as those with $\epsilon = 0\%$. The rate of cloud coalescence undergoes an increase at the time of initial close approach, but does not undergo a second increase at the time of merging.

The conversion of gas into stars makes the rises in both the cloud-cloud collisional rates and \dot{M}_{ovlp} much less dramatic than they are when $\epsilon = 0\%$. Since the luminosity is $\propto \epsilon \dot{M}_{\text{ovlp}}$ its dependence on time, except for a scale factor, will be the same as that of \dot{M}_{ovlp} . At the time of initial close approach peak values of the luminosity $\sim 0.7 \times 10^{11} L_{\odot}$, $2 \times 10^{11} L_{\odot}$, and $2.6 \times 10^{11} L_{\odot}$ are reached for $\alpha = 2.45$, 1.45, and 0.45 respectively. The luminosity of the galaxy as a function of time for each of the values of α is shown in Fig. 33. At the time when the galaxies merge, the luminosity for each value of α undergoes a second increase of magnitude comparable to the first. After the galaxies merge the luminosity of the merger remnant has luminosity $\sim 0.5 \times 10^{11} L_{\odot}$, $1.25 \times 10^{11} L_{\odot}$, and $1.5 \times 10^{11} L_{\odot}$ for $\alpha = 2.45$, 1.45, and 0.45 respectively. The ratio of luminosity to gas mass is shown as a function of time in Fig. 34. At the time of initial close approach peak values of $\sim 25 L_{\odot}/M_{\odot}$, $80 L_{\odot}/M_{\odot}$, and $100 L_{\odot}/M_{\odot}$ are obtained for $\alpha = 2.45$, 1.45 and 0.45 respectively. When the galaxies merge, this ratio undergoes a second increase which is larger than the first; this is because even though the luminosities are comparable the total gas mass is being depleted by star formation. It reaches a value of $25 L_{\odot}/M_{\odot}$, $100 L_{\odot}/M_{\odot}$, and $125 L_{\odot}/M_{\odot}$ for $\alpha = 2.45$, 1.45, and 0.45 respectively. As gas is continually being

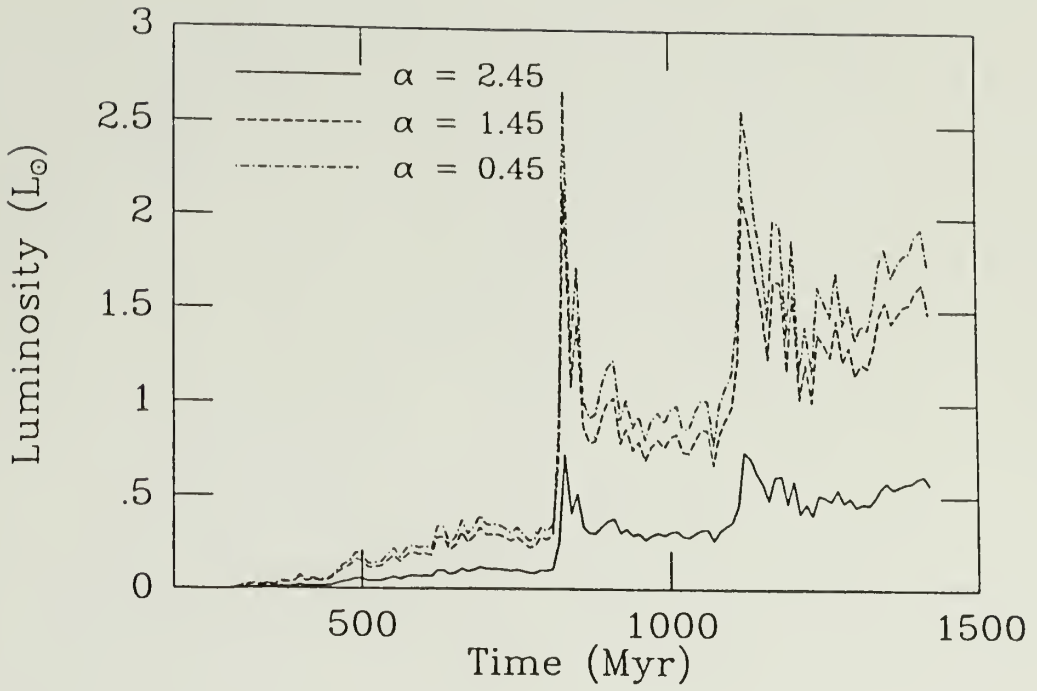


Figure 33 The luminosity of the galaxies as a function of time for case 8 where both galaxies contain gas.

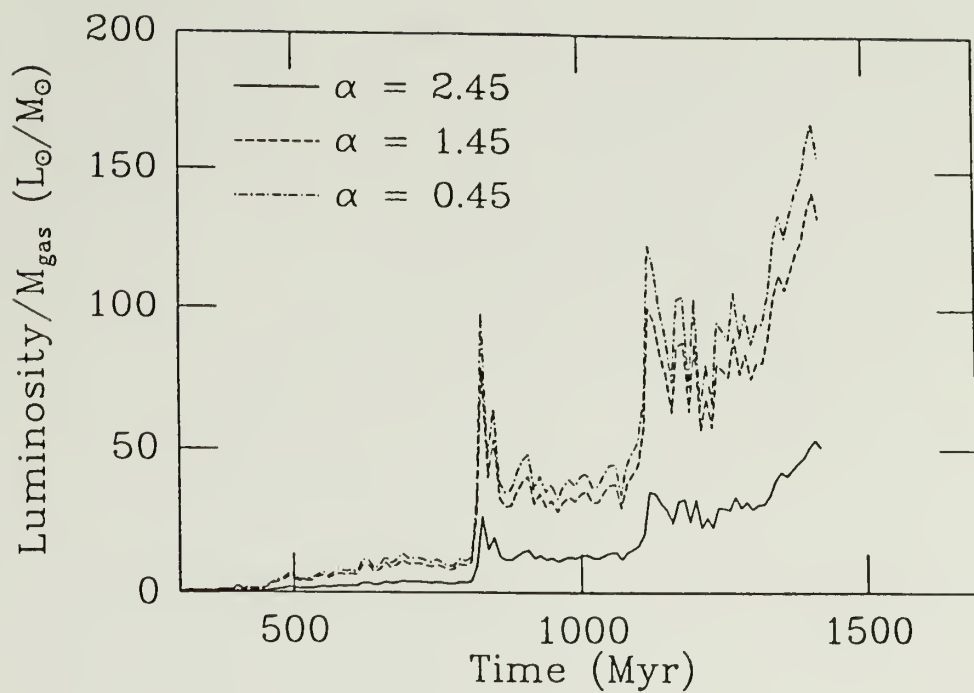


Figure 34 The luminosity to gas mass ratio as a function of time for case 8 taking into account the depletion of gas due to star formation.

depleted while the luminosity remains fairly steady after the galaxies merge, the luminosity to gas mass ratio rises to a value of $\sim 50 L_{\odot}/M_{\odot}$, $140 L_{\odot}/M_{\odot}$, and $170 L_{\odot}/M_{\odot}$ for $\alpha = 2.45$, 1.45 , and 0.45 respectively, toward the end of the calculation.

The largest observed value of $L_{\text{IR}}/M_{\text{H}_2}$ obtained by Solomon and Sage (1988) is $121 L_{\odot}/M_{\odot}$ for Mrk 231. This value can be explained by the above results for case 8 provided the initial mass function of stars is fairly flat ($1.45 \leq \alpha \leq 0.45$). Solomon and Sage (1988) classify Mrk 231 as belonging to interaction type 3, which consists of interactions not believed to be mergers. This galaxy could represent a merger in its early stages, however, since optical prints show two tails but not two separate galaxies (see Sanders et al. 1987). I also note that since Mrk 231 is classified as a Seyfert galaxy a fraction of the infrared luminosity from this galaxy could be provided by a nonthermal source of radiation. The highest value of $L_{\text{IR}}/M_{\text{H}_2}$ among the mergers (type 4) in the sample of Solomon and Sage (1988) is $79 L_{\odot}/M_{\odot}$ for the galaxy Arp 220.

Since case 8 has twice the amount of gas of any of the previous cases there is the possibility that the higher values of the luminosity to gas mass ratio obtained are the result of the larger mass of gas and not due to the circumstances that both galaxies contain gas and the galaxies merge. To investigate this, case 8 was rerun with $\frac{1}{2}$ the mass of gas. With the same initial cloud mass spectrum this meant that the number of clouds in each galaxy was halved. The star formation efficiency was set at $\epsilon = 20\%$. This case is labeled case 9. The evolution of the luminosity to gas mass ratio for case 9 is shown in Fig. 35.

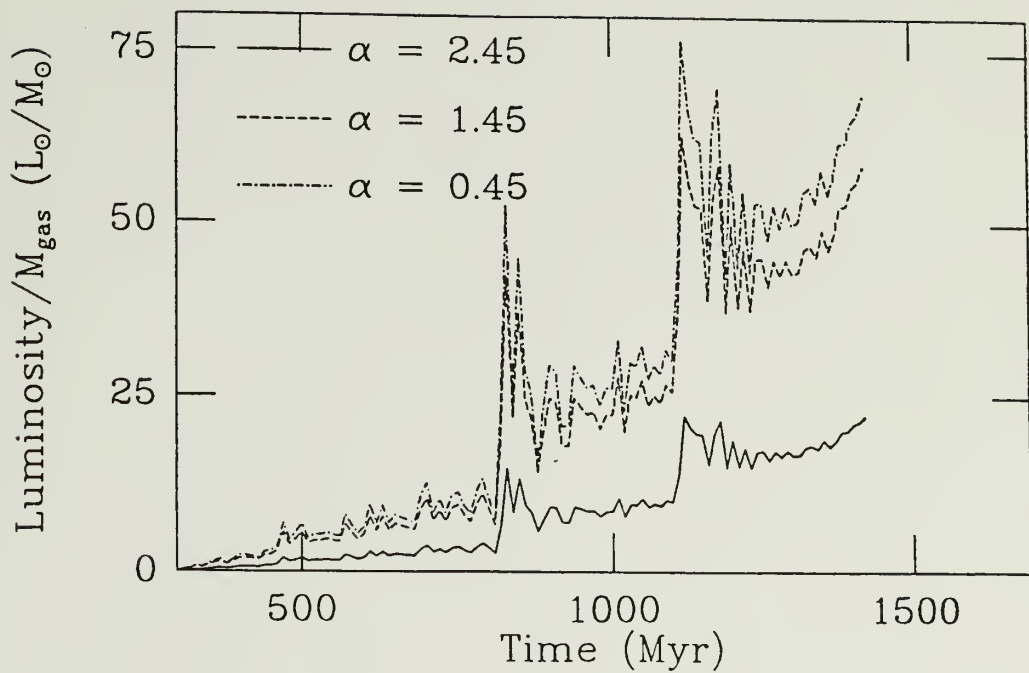


Figure 35 The luminosity to gas mass ratio as a function of time for case 9 where the total amount of gas is one half that in case 8 and both galaxies contain gas.

Cases 6 and 9 (i.e. Figs. 11 and 13) are first compared. The two cases differ in that the gas clouds all belong to one galaxy in case 6 while they are equally divided between the two galaxies in case 9. In the following discussion the situation of $\alpha = 1.45$ is considered. At the time of initial close approach, the luminosity to gas mass ratio rises to a value of $\sim 57 L_{\odot}/M_{\odot}$ in case 6, while this ratio is $\sim 43 L_{\odot}/M_{\odot}$ in case 9. Thus the ratio is higher, by a factor of 1.3, in case 6 owing to the higher spatial density of clouds, leading to more cloud-cloud collisions. At the time when the galaxies merge, however, the luminosity to gas mass ratio reaches a peak value $\sim 62 L_{\odot}/M_{\odot}$ in case 9, while it is only $\sim 40 L_{\odot}/M_{\odot}$ in case 6. Thus the merging of the two galaxies, causing the gas clouds in one galaxy to collide with those in the other, is instrumental in raising the luminosity to gas mass ratio.

The difference between cases 9 and 8 is that case 8 has twice the amount of gas. The higher spatial density of clouds in case 8 should then lead to a higher cloud-cloud collisional rate. Indeed the luminosity to gas mass ratio for case 8 exceeds that for case 9 by a factor of $\sim 1.5 - 2.0$ during the galaxy-galaxy interaction. From these comparisons of cases 6, 8, and 9 it is determined that the extremely high luminosity to gas mass ratio obtained in case 8 is due in part to the increased total amount of gas and in part to the circumstances that the galaxies merge and both galaxies contain gas.

CHAPTER 5

SUMMARY

The stronger the interaction of two galaxies the more disturbed the interstellar medium becomes. This manifests itself as an increase in the rate at which cloud-cloud collisions occur and in a larger fraction of the collisions producing disruption of the clouds. On the other hand, no large increase in the rate at which massive clouds are built up is found in any of the models described in this dissertation. As the strength of the interaction between two galaxies increases, the region of highest activity in the cloud system also becomes more and more concentrated toward the center of that galaxy.

It is suggested that most of the star formation which is induced by the interaction or merger of two galaxies is related to the high energy, disruptive cloud-cloud collisions which appear after the close passage of the two galaxies. These conditions under which stars form are not unlike those believed to be present during the early phase of the formation of a galaxy. By determining the star formation rate from the amount of mass overlapping in disruptive cloud-cloud collisions and taking the efficiency of star formation in the overlap regions as a parameter, it is found that, in order to produce the observed infrared luminosity to gas mass ratio, the efficiency of star formation is $\epsilon \gtrsim 20\%$ and the IMF of newly formed stars may be weighted toward higher mass stars than that in a

quiescent galaxy. This conclusion is somewhat uncertain in that a fraction of the observed infrared luminosity could be contributed by a non-thermal continuum source and in the case of a merger there may be a delayed burst of star formation owing to the build up of massive clouds in the nucleus.

It is also found that the formation of a bar due to the interaction of two galaxies is not a necessary prerequisite for nuclear star formation activity to be induced in the galaxy. It is also argued that a strong, long-lived bar may not be a preferred outcome of the tidal interaction between two galaxies since disk galaxies typically have rotation curves which are flat at least over 75 percent of the optical disk while the simulations of Noguchi (1988) which do form a strong, long-lived bar are those with rotation curves which become flat only beyond one half of the disk radius.

The effects of several parameters have also been considered. As the inclination of the interaction is increased the perturbation of the cloud system is decreased. This is reflected in both the morphological changes associated with the interaction and in the number of cloud-cloud collisions which are induced. Bound and unbound orbits have also been considered. Unbound orbits produce a smaller perturbation than bound orbits. Decreasing the mass of the perturbing galaxy also decreases the perturbation, as expected. The effect of having gas in both galaxies in an interaction in which the galaxies merge was also studied. Between the case in which both galaxies contain gas and that in which the same total amount of gas is located in one galaxy, a higher rate of disruptive cloud-cloud

collisions and therefore a higher $L_{\text{IR}}/M_{\text{H}_2}$ ratio is produced in the former case upon the merging of the galaxies. Increasing the total amount of gas in a given galaxy-galaxy interaction increases the initial spatial density of clouds, leading to higher cloud-cloud collision rates and higher $L_{\text{IR}}/M_{\text{H}_2}$ ratios. Indeed the highest observed value of $L_{\text{IR}}/M_{\text{H}_2}$ can be reproduced in one case calculated here in which the galaxies merge ($\gamma = 1/2$) and each galaxy contains $1.5 \times 10^9 M_{\odot}$ of gas, provided the IMF is relatively flat ($\alpha \geq 1.45$).

It has also been shown that while strong interactions between galaxies produce enhanced star formation rates at or near the nuclei of the galaxies, when the interaction is relatively weak (i.e. high γ or low mass of the perturbing galaxy) star formation can be induced in the outer regions of a galaxy with the nucleus remaining unaffected.

BIBLIOGRAPHY

- Aguilar, L. A., and White, S. D. M. 1986, *Ap. J.*, 307, 97.
- Alcock, C., and Pacynski, B. 1978, *Ap. J.*, 223, 244.
- Arp, H.C. 1966, *Atlas of Peculiar Galaxies* (Pasadena: California Institute of Technology).
- Barnes J. E. 1988, *Ap.J.*, 331, 699.
- Barnes, J., and Hut, P. 1986, *Nature*, 324, 446.
- Brunish, W. M., and Truran, J. W. 1982, *Ap. J. Suppl.*, 49, 447.
- Bushouse, H. A. 1986, Ph.D. thesis, University of Illinois.
- Bushouse, H. A., Lamb, S. A., and Werner, M. W. 1988, *Ap. J.*, 335, 74.
- Ezer, D., and Cameron, A.G.W. 1965, *Can. J. Phys.*, 43, 1497.
- _____ 1967, *ibid.*, 45, 3429.
- Fabbiano, G., Feigelson, E., and Zamorini, G. 1982, *Ap. J.*, 256, 397.
- Farouki, R. T., and Shapiro, S. L. 1982, *Ap. J.*, 259, 103.
- Fry, J. N., and Peebles, P. J. E. 1980, *Ap. J.*, 236, 343.
- Gilden, D. L. 1984, *Ap. J.*, 279, 335.
- Gott, J. R. 1977, *Ann. Rev. Astr. Ap.*, 15, 235.
- Harwit, M., and Fuller, C. E. 1988, *Ap. J.*, 328, 111.
- Iben, I. 1965, *Ap. J.*, 142, 1447.
- _____ 1966a, *ibid.*, 143, 483.
- _____ 1966b, *ibid.*, 505.
- _____ 1966c, *ibid.*, 516.
- _____ 1967, *ibid.*, 147, 624.
- Jackson, J. D. 1975, *Classical Electrodynamics 2nd ed.*, (New York: Wiley), p. 137.
- Joseph, R. D., and Wright, G.E. 1985, *M.N.R.A.S.*, 214, 87.
- Kennicutt, R.C., and Keel, W.C. 1984, *Ap. J.*, 279, L5.

- Kennicutt, R. C., Keel, W. C., van der Hulst, J. M., Hummel, E., and Roettiger, K. A. 1987, *A. J.*, **93**, 1011.
- Kwan, J., and Valdes, F. 1987, *Ap. J.*, **315**, 92.
- Lamb, S. B., Iben, I. and Howard, W. M. 1976, *Ap. J.*, **207**, 209.
- Latanzio, J. C., and Henriksen, R. N. 1988, *M.N.R.A.S.*, **232**, 565.
- Larson, R. B., and Tinsley, B. M. 1978, *Ap. J.*, **219**, 46.
- Lonsdale, C. J., Persson, S. E. and Mathews, K. 1984, *Ap. J.*, **287**, 95.
- McGlynn, Thomas A. 1984, *Ap. J.*, **281**, 13.
- Meyer-Hofmeister, E. 1972, *Astr. Ap.*, **16**, 282.
- Noguchi, M. 1988, *Astr. Ap.*, **203**, 259.
- Noguchi, M., and Ishibashi, S. 1986, *M.N.R.A.S.*, **219**, 305.
- Rieke, G. H. 1988, *Ap. J.*, **331**, L5.
- Rubin, V. C., Burstein, D., Ford, W. K. and Thonnard, N. 1985, *Ap. J.*, **289**, 81.
- Sanders, D. B., Scoville, N. Z., Young, J. S., Soifer, B. T., Schloerb, F. P., Rice, W. L. and Danielson, G. E. 1986, *Ap. J.*, **305**, L45.
- Sanders, D. B., Young, J. S., Scoville, N. Z., Soifer, B. T., and Danielson, G. E. 1987, *Ap. J.*, **312**, L5.
- Scalo, J. M., and Struck-Marcell, C. 1986, *Ap. J.* **301**, 77.
- Searle, L., Sargent, W. L. W., and Bagnuolo, W. G. 1973, *Ap. J.*, **179**, 427.
- Sellwood, J. A. 1987, *Ann Rev. Astr. Ap.*, **25**, 151.
- Smith, B. 1988, Ph.D. dissertation, University of Massachusetts.
- Solomon, P. M., and Sage L. J. 1988, *Ap. J.*, **334**, 613.
- Toomre, A. 1964, *Ap. J.*, **139**, 1217.
- Toomre, A., and Toomre, J. 1972, *Ap. J.*, **178**, 623.
- Vandenberg, D. A. 1985, *Ap. J. Suppl.*, **58**, 711.
- Vásquez, E. C., and Scalo, J. M. 1989, *Ap. J.*, **343**, 644.

- Villumsen, J. V. 1982, *M.N.R.A.S.*, **199**, 493.
- Wagner, R. L. 1974, *Ap. J.*, **191**, 173.
- White, R. L. 1988, *Ap. J.*, **330**, 26.
- White, S. D. M. 1983, *Ap. J.*, **274**, 53.
- Young, J. S., Kenney, J. D., Tacconi, L., Claussen, M. J., Huang, Y.-L., Tacconi-Garman, L., Xie, S. and Schloerb, F. P. 1986b, *Ap. J.*, **311**, L17.
- Young, J. S., Schloerb, F. P., Kenney, J. D. and Lord, S. D. 1986a, *Ap. J.*, **304**, 443.

